A critical thermal transition driving spring phenology of Northern Hemisphere conifers

A critical thermal transition driving spring phenology of Northern Hemisphere conifers

Running Head: Thermal transition and phenology

Jian-Guo Huang[1*], Yaling Zhang[2*], Minhuang Wang[3], Xiaohan Yu[4], Annie Deslauriers[5], Patrick Fonti[6], Eryuan Liang[7], Harri Mäkinen[8], Walter Oberhuber[9], Cyrille B. K. Rathgeber[10], Roberto Tognetti[11], Václav Treml[12], Bao Yang[13], Lihong Zhai[2], Jiao-Lin Zhang[14], Serena Antonucci[11], Yves Bergeron[15], J. Julio Camarero[16], Filipe Campelo[17], Katarina Čufar[18], Henri E. Cuny[19], Martin De Luis[20], Marek Fajstavr[21], Alessio Giovannelli[22], Jožica Gričar[23], Andreas Gruber[9], Vladimír Gryc[21], Aylin Güney[24, 25], Tuula Jyske[8], Jakub Kašpar[12, 26], Gregory King[6, 27], Cornelia Krause[5], Audrey Lemay[5], Feng Liu[28], Fabio Lombardi[29], Edurne Martinez del Castillo[20], Hubert Morin[5], Cristina Nabais[17], Pekka Nöjd[8], Richard L. Peters[6, 30], Peter Prislan[18], Antonio Saracino[31], Vladimir V. Shishov[32], Irene Swidrak[9], Hanuš Vavrčík[21], Joana Vieira[17], Qiao Zeng[33], Yu Liu[34‡], and Sergio Rossi[5]

Affiliations:

[1] Key Laboratory of Conservation Biology for Endangered Wildlife of the Ministry of Education, College of Life Sciences, Zhejiang University, Hangzhou, China

[2] Key Laboratory of Vegetation Restoration and Management of Degraded Ecosystems, Guangdong Provincial Key Laboratory of Applied Botany, South China Botanical Garden, Chinese Academy of Sciences, 723 Xingke Road, Tianhe District, Guangzhou, 510650, China

[3] Department of Ecology, School of Life Sciences, State Key Laboratory of Biocontrol, Sun Yat-sen University, Guangzhou, 510275, China

[4] School of Engineering and Built Environment, Griffith University, 170 Kessels Road, Nathan, Brisbane, 4111, Australia

[5] Laboratoire sur les écosystèmes terrestres boréaux, Département des Sciences Fondamentales, Université du Québec à Chicoutimi, Chicoutimi (QC), Canada

[6] Swiss Federal Research Institute for Forest, Snow and Landscape Research WSL, Zürcherstrasse 111, CH-8903 Birmensdorf, Switzerland

[7] Key Laboratory of Alpine Ecology and Biodiversity, Key Laboratory of Tibetan Environment Changes and Land Surface Processes, Institute of Tibetan Plateau Research, Chinese Academy of Sciences, Beijing, China

[8] Department of Forests, Natural Resources Institute Finland, Espoo, Finland

[9] Department of Botany, Leopold-Franzens-University of Innsbruck, Innsbruck, Austria

[10] Université de Lorraine, AgroParisTech, INRAE, Silva, F-54000 Nancy, France

[11] Dipartimento di Agricoltura, Ambiente e Alimenti, Università degli Studi del Molise, Campobasso, 86100, Italy

[12] Department of Physical Geography and Geoecology, Charles University, Prague, CZ-12843, Czech Republic

[13] Cold and Arid Regions Environmental and Engineering Research Institute, Chinese Academy of Sciences, China 730000

[14] CAS Key Laboratory of Tropical Forest Ecology, Xishuangbanna Tropical Botanical Garden, Chinese Academy of Sciences, Mengla, Yunnan, 666303, China

[15] Forest Research Institute, Université du Quebec en Abitibi-Témiscamingue, Rouyn-Noranda, Quebec, Canada J9X5E4

[16] Instituto Pirenaico de Ecología (IPE-CSIC), Avda. Montañana 1005, Zaragoza, 50192, Spain

[17] Centre for Functional Ecology, Department of Life Sciences, University of Coimbra, Calçada Martim de Freitas, Coimbra, 3000–456, Portugal

[18] University of Ljubljana, Biotechnical Faculty, Ljubljana, Slovenia

[19] IGN, Direction Interrégionale NordEst, Champigneulles, France

[20] Department of Geography and Regional Planning, Environmental Science Institute, University of Zaragoza, Zaragoza, 50009, Spain

[21] Department of Wood Science and Wood Technology, Mendel University in Brno, Zemědělská 3, Brno, 61300, Czech Republic

[22] CNR – Istituto di Ricerca sugli Ecosistemi Terrestri, IRET, Sesto Fiorentino, Italy

[23] Slovenian Forestry Institute, Ljubljana, Slovenia

[24] Institute of Botany, University of Hohenheim, Germany

[25] Southwest Anatolia Forest Research Institute, Antalya, Turkey

[26] Silva Tarouca Research Institute for Landscape and Ornamental Gardening, Department of Forest Ecology, 252 43 Průhonice, Czech Republic

[27] Department of Sciences, University of Alberta, Camrose, AB, Canada

[28] Key Laboratory of Aquatic Botany and Watershed Ecology, Wuhan Botanical Garden, Chinese Academy of Sciences, Wuhan 430074, China

[29] AGRARIA Department, Mediterranean University of Reggio Calabria, 89124, Italy

[30] Laboratory of Plant Ecology, Department of Plants and Crops, Faculty of Bioscience Engineering, Ghent University, Coupure links 653, B-9000 Ghent, Belgium

[31] Department of Agricultural Sciences, University of Naples Federico II, I-80055

Portici-Napoli, Italy

[32] Institute of Economics and Trade, Siberian Federal University, Krasnoyarsk, 660075, Russia

[33] Key Lab of Guangdong for Utilization of Remote Sensing and Geographical Information System, Guangdong Open Laboratory of Geospatial Information Technology and Application, Guangzhou Institute of Geography, Guangzhou 510070, China

[34] The State Key Laboratory of Loess and Quaternary Geology, Institute of Earth Environment, Chinese Academy of Sciences, 710061 Xi'an, China

[*] These authors contributed equally to this work.

[‡] To whom correspondence may be addressed.

Yu Liu

Email: liuyu@loess.llqg.ac.cn

Abstract

Despite the growing interest in predicting shifts in plant phenology to climate change, advanced spring phenology by global warming remains open for debate. Evidence documenting either small or large advancement of spring phenology to rising temperature over the spatio-temporal scales implies a potential existence of a thermal threshold in the responses of forests to global warming. We collected a unique dataset of xylem cell-wall-thickening onset dates in 20 coniferous species covering a broad mean annual temperature (MAT) gradient (-3.05 to 22.9°C) across the Northern Hemisphere (latitudes 23-66°N). We fit a generalized segmented regression model with one breakpoint (AIC=17274.2 and BIC=17302.2) that outperformed a generalized linear regression (AIC=17326.0 and BIC=17342.8). Such a result supported our hypothesis of a thermal transition. We identified a threshold temperature of 4.9±1.1°C along the MAT gradient, above which the response to rising temperature would significantly decline. This threshold segregates the Northern hemisphere conifers into cold and warm thermal niches, with MAT and spring forcing being the main drivers for the onset dates, respectively. The identified thermal threshold should be integrated into the Earth-System-Models for an improved prediction of global carbon and energy cycles under global warming.

Keywords:

xylem phenology, cell-wall-thickening, photoperiod, spring forcing, winter chilling, Northern Hemisphere conifer

Introduction

As an integrated response to the environmental changes, forest spring phenology is interconnected with ecosystem functions and services, including forest productivity (Cuny et al., 2015), species distribution (Kharouba et al., 2018), and community assemblage (Piao et al., 2019). The advances in spring phenology commonly observed as a major imprint of climate change impacts across all

biomes have received much attention (Menzel et al., 2006; Richardson et al., 2013), but are mostly focused on the onset of primary growth (Delpierre et al., 2016). Secondary growth, or xylem phenology, has been neglected until the development of the microsampling approach (Deslauriers, Morin, & Begin, 2003). Temperature has been widely recognized as a key driver for cambial reactivation of northern hemisphere conifers (Huang et al., 2020; Rossi et al., 2016). Warmer temperatures promote hormone production and the conversion of starch to sugar, thus breaking the dormancy (i.e., ecodormancy) and inducing cell division in the vascular cambium (Begum et al., 2018). These processes have been confirmed from experiments of localized heating of the stem (Oribe et al., 2003) and field observations of wood formation (Moser et al., 2010; Rossi et al., 2016). More recently, studies on the onset of primary growth have demonstrated the declining effects of global warming on spring phenology, indicating a slowdown in the advancement of spring phenology, especially in warm ecosystems (Fu et al., 2015; Vitasse et al., 2018). For instance, larger advancements of spring phenology have been observed at higher altitudes, colder sites, and rural areas (Meng et al., 2020; Prevéy et al., 2017; Vitasse et al., 2018). Such differences in the advancing rates raise questions about the occurrence of critical thresholds along thermal gradients above which the process of advancement decreases significantly. However, despite the ecological importance of a potential transition temperature in shaping terrestrial biomes with climate warming, it has not been accurately incorporated in global models (Delpierre et al., 2019; Huang et al., 2020), which jeopardizes the model's performance in predicting phenological responses under future climate scenarios.

Trees require a sufficient forcing temperature above a threshold of 0-5°C for the resumption of xylem growth (Antonucci et al., 2015). On one hand, a warming can accelerate the advancing rate through the accumulation of forcing temperature. On the other hand, warming impose a higher forcing temperature requirement through the lower accumulation of chilling (i.e., the sum of low temperature

incidents informing that winter has passed) (Asse et al., 2018; Delpierre et al., 2019). Such a dual effect of warming could play a role in slowing down the advancement of spring phenology under warming conditions (Delpierre et al., 2019; Meng et al., 2020; Montgomery et al., 2020). Growth reactivation is also controlled by photoperiod over the northern hemisphere (Huang et al., 2020; Rossi et al., 2016). Photoperiod could constrain the advancement under warming conditions as spring phenological events tends to occur at a shorter photoperiod (Fu et al., 2019; Meng et al., 2020). Despite the numerous hypotheses raised in the literature, the factors involved in the reduction of the advancement of tree spring phenology remains to be disentangled.

Herein, we aimed to identify the threshold temperature at which the advancement of spring phenology to rising temperature drop significantly, and to elucidate the possible causes of the decline. “Space-for-time-approach” is widely used in ecology for inference about future climate change impacts (Elmendorf et al., 2015; Peters et al., 2019). One previous study showed that there is virtually no spatial bias for predicting the timing of cambial resumption (Delpierre et al., 2019). They suggest that the spring onset of wood formation is far less affected by the species and the large environmental gradients. These findings were confirmed by another study showing that species and site were not the main factor affecting the onset of wood formation of conifers across the northern hemisphere (Huang et al., 2020). Thus, with a scarcity of high-quality time series in xylem phenology, applying a space-for-time approach could be a reasonable alternative to project the impacts of climate change for wood phenology (Rossi et al., 2016). We therefore proposed that the spatial pattern of the onset dates of xylem phenological activities along the gradient of MAT revealed in our study can provide a framework to examine the responses of secondary growth of forests to rising temperatures.

In this study, we compiled a large and unique dataset of weekly cell-wall-thickening phenological measurements of 20 coniferous species from 75

sites over the Northern Hemisphere as surrogates for spring phenological activity. These sites spanned across a broad mean annual temperature (MAT) gradient (-3.05°C to 22.9°C), from 23°11' N to 66°12' N, including boreal, temperate, Mediterranean, and subtropical biomes (Fig. 3a and table S1). The cell-wall-thickening process is part of the secondary growth of trees representing the progression from cell-enlargement to cell-wall-thickening, lignification, and programmed cell death that generates the mature xylem (fig. S1) (Begum et al., 2013). This process ultimately accounts for 90% of the woody biomass production of forest trees (Cuny et al., 2015). Thus, weekly cell-wall-thickening phenological measurements offer a unique opportunity to describe the dynamics of the global carbon cycle and improve our ability to simulate the future of the Earth's system at a high temporal resolution.

Materials and Methods

Field experiments and sample collection

Xylogenesis was monitored throughout the growing season from January–April to October–December according to the local climate of the sites. The monitoring years varied among the sampling sites from 1998 to 2016 (table S1). At each site, from 1 to 55 adult dominant trees with upright, healthy trunks were selected for sampling. Wood microcores (2.5 mm in diameter × 25 mm long) were collected weekly (90%) or, on occasion, biweekly, from around the stems at breast height (1.3±0.3 m) using a Trephor microcorer (Rossi et al., 2006). The samples usually contained several (or at least one) previous tree rings, as well as the developing annual layer with the cambial zone and adjacent phloem tissues. The microcores were stored immediately at 5°C in solutions of propionic or acetic acid mixed with formaldehyde or ethanol to avoid tissue deterioration and were then transported to the lab for further treatment. The microcores were dehydrated in ethanol and *D*-limonene and then embedded in paraffin or glycol methacrylate. Transverse sections 10–30 µm thick were cut from the samples with rotary or sledge microtomes. Sections were stained with aqueous cresyl violet acetate or double-

stained with safranin and astra blue and observed with bright-field and polarized light to differentiate the developing xylem cells.

In total, data were collected from 814 individuals of 20 conifers distributed across 75 sites that covered boreal, temperate, Mediterranean, and subtropical biomes in North America, Europe, and Asia. The sites were distributed over latitudes from 23°11' N to 66°12' N and at elevations ranging from 23 m to 3850 m a.s.l. (Fig. 3a and table S1).

Species classification

Early successional species are the shade-intolerant pioneers corresponding to life history strategies of fast growth rate and an ability to grow in harsh conditions, whereas late successional species are those that are shade tolerant and characterized by a slow growth rate. There were 645 individuals belonging to the early successional species, i.e. *Juniperus przewalskii* (JUPR), *Juniperus thurifera* (JUTH), *Larix decidua* (LADE), *Pinus halepensis* (PIHA), *Pinus heldreichii* (PIHE), *Pinus leucodermis* (PILE), *Pinus longaeva* (PILO), *Pinus massoniana* (PIMA), *Pinus peuce* (PIPE), *Pinus pinaster* (PIPI), *Pinus sylvestris* (PISY), *Pinus tabulaeformis* (PITA), *Pinus uncina* (PIUN). There were 1302 individuals belonging to the late successional species, i.e. *Abies alba* (ABAL), *Abies balsamea* (ABBA), *Abies georgei* (ABGE), *Cedrus libani* (CELI), *Picea abies* (PCAB), *Picea mariana* (PCMA), *Pinus cembra* (PICE). In general, the two successional species overlap along the MAT gradients, except the individuals of the early successional species located at warmer sites (Fig. 1b). Three species, JUPR, JUTH, and PIHE, are unique species that grow in harsh conditions, show a slow growth rate and a long-life history. They cannot be grouped into early or late successional species according to classical theory therefore, they were excluded when splitting the data into different successional stages and associated downstream analyses.

Xylem phenology data

A common protocol for classifying xylem cells at different developmental phases was followed at all sites. For each sample, the number of cells in the cambial

zone, and cells in the enlargement and secondary cell wall thickening phases were counted along three radial rows. Thin-walled enlarging cells were distinguished from cambial cells by their larger size, as they had a radial diameter at least twice that of a fusiform cambial cell (Deslauriers et al., 2003). A wall-thickening cell was differentiated from an enlarging cell by the presence of a secondary cell wall that displayed birefringence under polarized light due to the orientation of the cellulose microfibrils (Abe et al., 1997).

Color changes from violet to blue (simple cresyl violet acetate staining) or from blue to red (double safranin-astra blue staining) demonstrated the entire progression of wall thickening (fig. S1). Mature cells presented entirely lignified, monochromatic walls, therefore, the absence of cytoplasm and a complete color change over the whole cell wall marked the end of lignification and the full maturation of the tracheid (Abe et al., 1997). The mean number of xylem cells in the wall-thickening phase was obtained at each sampling date. The timing of the onset of wall thickening, represented by the day of the year (DOY), was defined for each tree, site, and year as the date of appearance of the first wall-thickening cell and was referred to as the cell-wall-thickening DOY.

Statistical analyses

We also explored key drivers of cell-wall-thickening DOY among six selected common potential predictors (MAT, photoperiod, forcing, chilling, scPDSI, and spring temperature variation) using three classes of statistical models: boosted regression trees (BRTs), linear mixed effect models (LMMs), and Bayesian mixed-effects models (BMMs). We also performed a natural cubic spline to check for the general trends among different predictor variables or between the cell-wall-thickening DOY and a certain selected predictor.

General patterns: settings and diagnostics for BRTs

We assessed the relative importance of explanatory variables in predicting the cell-wall-thickening DOY using BRTs (fig. S2a), as these have been used

extensively in ecological studies with an ensemble of 'boosted' multiple decision trees for analysis of complex systems (Frey et al., 2016; McClanahan et al., 2019). The fitting procedures for a BRT model do not make assumptions on data distribution for a large dataset, and they have several advantages, such as collinearity handling among predictors and robustness to outliers (Elith et al., 2008), especially when accounting for nonlinear relationships and complex interactions between explanatory variables of multiple classes during boosted regression modeling (Venter et al., 2018). We used the following settings for our BRT model: a tree complexity of 10, a learning rate at 0.005, and a bag fraction of 0.7. A smaller learning rate corresponds to a higher number of trees used in the model, while the bag fraction was added as a stochastic component that improves model performance by reducing variance in the final model. A final BRT model with 5800 trees was chosen in our study.

A partial dependence plot following BRT modeling was then constructed to show the general trending pattern of the relationship between the cell-wall-thickening DOY and each predictor (fig. S2b-g). The R program packages "gbm" package, "dismo," and "pdp" were used for the BRT analyses and visualization (Muggeo, 2008).

After using the fitted BRT model to confirm MAT as the most important predictor (fig. S1a), we fitted a natural cubic spline (Ortiz-Bobea et al., 2018) to provide a nonlinear smoothed estimate of the other five predictors and frost frequency along the MAT gradient (fig. S3). Cubic spline regressions make no assumptions about the shape of a curve other than smoothness, and they are commonly suggested for examination of the fitness and performance of natural selection on a quantitative trait, such as the thermal performance traits (Logan et al., 2014). Cubic splines were estimated using the "mgcv" package.

Breakpoint analysis: cell-wall-thickening DOY versus MAT

The preliminary analyses described above revealed an apparent transition of the

relationship between cell-wall-thickening DOY and MAT from the BRT-related partial dependence plot (fig. S2b), indicating that the possible existence of a thermal transition along the MAT gradient. We conducted a methodology for threshold detection following (Berdugo et al., 2020). Specifically, we constructed generalized linear and segmented regressions to the relationships between cell-wall-thickening DOY and MAT with a log-linked Gaussian error distribution for the full dataset using the R package "MASS" and the 'Segmented' R package (Muggeo, 2008) (Fig. 1), respectively. We used AIC to decide the model that provided the best fit in each case (Hastie, 2017). This criterion lower than 2 indicates that the model is significantly better (Berdugo et al., 2020). Only when non-linear regressions were a better fit to the data, thresholds may be present. Therefore, we explored the presence of thresholds only when non-linear models were a better fit to the data. We fitted segmented regressions describing the point in the predictor (MAT) that evidences the shift in the relationship (in slope, intercept or slope + intercept) between cell-wall-thickening DOY and MAT. We consider a threshold as the point in MAT in which the cell-wall-thickening DOY changes abruptly its value.

Next, to confirm the significance of the cell-wall-thickening trends (for overall observations and species referring to each successional stage) before and after the identified breakpoint (estimated at 4.9±1.1℃), the full dataset was split into cold (≤4.9℃) and warm (＞4.9℃) temperature zones. Data in each temperature zone were obtained by further splitting into different sub-datasets according to their successional stages, that is, as early and late successional species.

Among the fitted segmented linear models, the statistical significance of the differences between the slopes of regressions was tested with standardized major axis estimation (SMA) (e.g., the difference in the regression slopes between temperature zones or successional stages) as implemented in the smatr R package (Fox & Weisberg, 2018). We also chose robust SMA estimation, which handles outliers with Huber's M-estimator, because our SMA approaches are highly sensitive to outliers (Warton et al., 2012). All analyses were performed in R

v.3.6.3 (Warton et al., 2012).

LMMs and BMMs settings and diagnostics

We further examined the direction and magnitude of the relationships between environmental predictors and site covariates with cell-wall-thickening DOY by fitting a linear mixed effect model and Bayesian mixed-effects model for both the overall dataset and the sub-datasets. Summary statistics (raw mean, median and quantiles) of all datasets were obtained (table S2) by fitting intercept-only LMMs without fixed predictor variables, using "site" and "species" as random intercept terms.

The LMMs were used to test for the main effects of the explanatory variables on cell-wall-thickening DOY. We obtained a best model for each dataset by performing model selection procedures to determine the best random-effects structure and the optimized fixed-effect structure through a backward stepwise model simplification, using all the explanatory variables in the fixed component for the most complex models (table S3). Collinearity among variables was detected by the variance inflation factor (vif), and the variables with vif <3 were retained. The most complex model was fitted using the following formula:

$$D_{ijk} = \alpha + \beta 1\mathrm{MAT}_{ijk} + \beta 2P_{ijk} + \beta 3F_{ijk} + \beta 4C_{ijk} + \beta 5PDSI_{ijk} + \beta 6\mathrm{Tem\_variation}_{ijk} + a_i + b_j + \varepsilon,$$

where D_{ijk} is the date of onset of the first cell wall thickening of species i at site j in year k; MAT_{ijk}, P_{ijk}, F_{ijk}, $C_{ijk,}$ $PDSI_{ijk}$, and $Tem\_variation_{ijk}$ are fixed effects and represent the mean annual temperature, photoperiod, forcing, chilling, scPDSI, and spring temperature variation corresponding to D_{ijk}, respectively; α is the intercept; β_1, β_2, $\beta_{3,}$ β_4, β_5, and β_6 are the slopes; a_i and b_j are the random effects of the site i and species j, respectively; and ε is the error term.

Log-likelihood ratio tests and *F* tests were used to perform backward elimination of non-significant random and fixed effects (Kuznetsova, Brockhoff, & Christensen, 2014) (table S3). In particular, the fixed effects were retained or

removed based on changes in the AIC, with ΔAIC values of <−2 as a criterion to drop variables and on a likelihood ratio test with a *P* value (based on Satterthwaite approximation) higher than 0.05, through which a rigorous estimate of the most parsimonious model was retained. The validity of the assumptions of normality and homoscedasticity was examined using residual plots (Burnham et al., 2011). For each optimal LMM, the contributions of the fixed- and random-effects variables in explaining variation in the dependent variable (i.e., cell-wall-thickening DOY) were calculated by a variance-partitioning analysis to partition the variances attributable to each variable into the best-fitting model (Hoffman & Schadt, 2016). We reported the coefficients of the optimal model estimated by the restricted maximum likelihood approach, the bootstrap confidence interval (90 and 95%) calculated based on 1,000 simulations, and the marginal and conditional R^2 values, which account for fixed and fixed plus random effects. All the statistical analyses associated with LMMs were conducted using the R packages lme4, MuMIn, and lmerTest.

The magnitude and significance of the six predictors in determining cell-wall-thickening DOY were further examined by BMMs. The selected models were similar to those obtained by LMMs. We standardized and centered the numerical independent variables before analyses, thereby facilitating the direct comparison of the resulting coefficients. All explanatory variables were considered in these models, which we ran as four chains with 2000 iterations each, burning 1000 samples per chain, with analysis of 1000 post-warmup samples. Statistical significance was obtained by means of the posterior distribution of the 95% credible interval of its mean estimate (log odds ratio). Positive and negative values of the log odds ratio denote positive versus negative effects, respectively, while a significant effect occurs when no overlap exists between the 95% error bars and zero.

Results

Thermal transition across temperature (MAT) gradient

We identified MAT as the major driver of cell-wall-thickening DOY among selected predictors with boosted regression tree (BRT) analyses (fig. S2a). Partial dependence plot from BRT further showed that cell-wall-thickening DOY was a decreasing function of the rising MAT gradient (i.e., phenological advance) and responded in a nonlinear manner, with apparent thermal transitions along the descending trend (fig. S2b). A generalized segmented regression model assuming one breakpoint (AIC=17274.2 and BIC=17302.2) outperformed a generalized linear regression (AIC=17326.0 and BIC=17342.8) and supported such a hypothesized thermal transition. Observed temperature-scaling of the cell-wall-thickening DOY based on the piecewise model indicates a qualitative transition at MAT=4.9±1.1℃ (Fig.1a). The slopes of the segments to the left (-5.14) and to the right (-2.89) of the observed breakpoint differed significantly (Davies' test, $P = 0.001$). Consequently, this thermal transition separated our study sites into the cold and the warm ecosystems, whereby a significantly greater phenological advancement occurred in sites with MAT below 4.9 °C but a smaller advancement occurred in sites with MAT above 4.9 °C, respectively (Fig. 1a, b).

Accordingly, species with sufficient coverage along the MAT gradient, e.g. *Picea abies* (n= 447, fig. S4), exhibited a significantly greater advancement in cold regions and a smaller advancement in warm areas (fig. S5; $P = 0.001$). At the biome level, both boreal and cold-temperate forests (MAT <4.9°C) showed a significantly stronger advancement than did Mediterranean and warm-temperate forests (MAT >4.9°C) (fig. S6; $P = 0.001$). Previous studies have reported that early successional species are more responsive to rising temperature than are the late successional ones (13, 15), and therefore, we also considered them separately in the current study (see Species classification in Materials and Methods for further details). The early and late successional species also revealed similar patterns, that is, have smaller advancement when MAT >4.9°C (Fig. 1b).

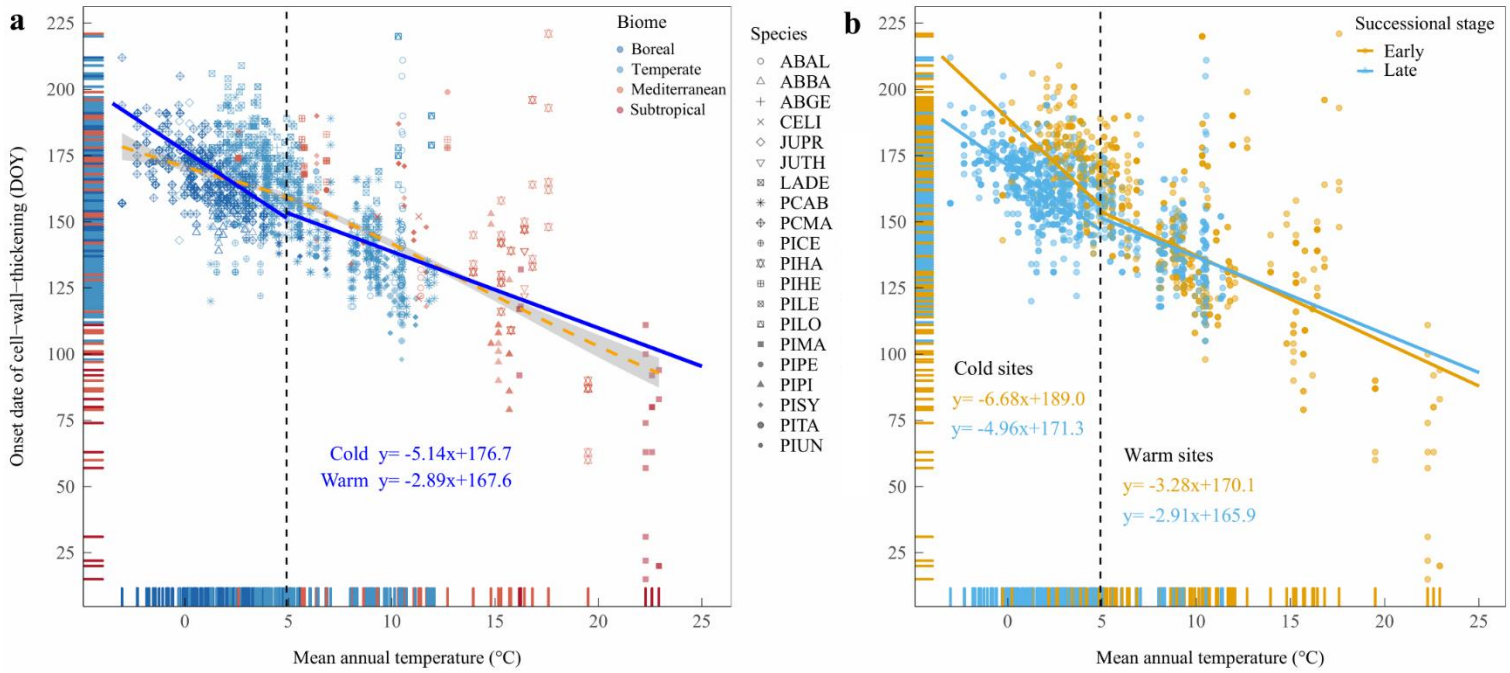

Fig 1. Changes in the cell-wall-thickening DOY (day of the year) along the mean annual temperature (MAT) gradients of the study sites separate contrasting slopes between cold and warm sites. According to the determined break point (at 4.9±1.1℃), segmented regression lines (the solid lines) were fitted with linear mixed-effect models separately for all observations (a) and for early successional species and late successional species (b) at different temperature zones. The dashed orange line (a) was fitted with a generalized linear model for all observations. Species are reported with the following acronyms and classified into early (JUPR, *Juniperus przewalskii*; JUTH, *Juniperus thurifera*; LADE, *Larix decidua*; PIHA, *Pinus halepensis*,; PIHE, *Pinus heldreichii*; PILE, *Pinus leucodermis*; PILO, *Pinus longaeva*; PIMA, *Pinus massoniana*; PIPE, *Pinus peuce*; PIPI, *Pinus pinaster*; PISY, *Pinus sylvestris*; PITA, *Pinus tabulaeformis*; and PIUN, *Pinus uncina*) and late (ABAL, *Abies alba*; ABBA, *Abies balsamea*; ABGE, *Abies georgei*; CELI, *Cedrus libani*; PCAB, *Picea abies*; PCMA, *Picea mariana*; PICE, *Pinus cembra*) successional species types ((see (47) for further details)). Points (n=1948) represent individual trees from the 75 study sites included in this study. Biomes include boreal (B), temperate (T), Mediterranean (M), and subtropical (S).

The partition of variance of the main drivers

By constructing linear mixed effect models (LMMs) and Bayesian mixed-effects models (BMMs), we explored the reasons underlying the decreased advancement to rising temperature and assessed and quantified the main environmental drivers for the onset of cell-wall-thickening in cold versus warm ecosystems (see LMMs and BMMs settings and diagnostics in Statistical analyses for further details). The onset of the spring phenology of forest trees is also strongly regulated by local spring temperature variance and soil moisture availability (Huang et al., 2020; Körner & Basler, 2010), and these parameters were included in the LMMs and BMMs.

In the cold sites, MAT remained as the main driver for the cell-wall-thickening DOY, while its relative importance substantially decreased in warm sites, where forcing superseded MAT as the major driver (Fig. 2a, b, g). In determining the cell-wall-thickening DOY, photoperiod was more important in warm sites than in cold sites (Fig. 2 a, b, g). Similarly, chilling consistently explained higher variances of cell-wall-thickening DOY in warm sites than that in cold sites (Fig. 2 a, b, g).

In addition, the relative importance of selected phenological predictors differed between different successional stages, i.e., early- versus late-successional species. MAT in regulating cell-wall-thickening DOY explained a higher variance for both early and late species in cold sites than in warm sites, especially for the early ones. Similarly, photoperiod was more important for the early species than the late species in warm sites (Fig. 2c, d, e, f, g). Higher scPDSI delayed the cell-wall-thickening DOY, again more pronounced for the early species (Fig. 2 c, d, e, f, g).

At the biome level, MAT played a much more important role in determining cell-wall-thickening DOY in the boreal and cold-temperate forests than in the Mediterranean and warm-temperate forests (fig. S7). By contrast, forcing was the dominant driver for the Mediterranean and warm-temperate forests (fig. S7).

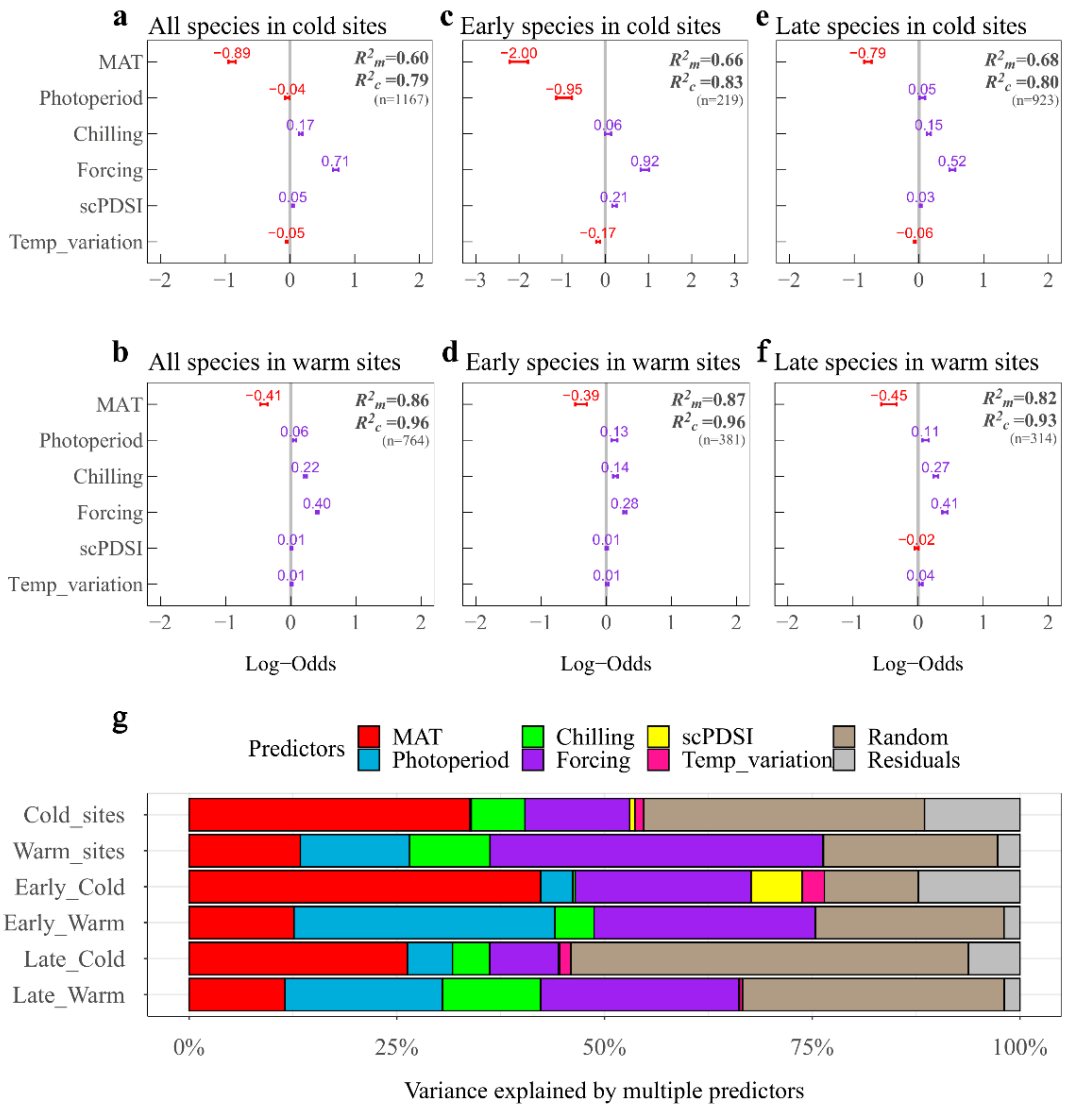

Fig 2. Summary of the direction and magnitude of the effect of all predictors on cell-wall-thickening DOY (day of the year) in different systems using Bayesian linear mixed effect models, shown in a-f, and including samples from different temperature zones: the upper (a, c, e) and lower (b, d, f) panels were from cold and warm sites, respectively. Samples were also assigned to different successional stages: early species (c, d) and late species (e, f). Significant effects occur when no overlaps exist between the 95% error bars and zero. The blue and red colors denote positive versus negative effects, respectively. The Bayes factors are provided to show significance. Marginal and conditional R squared (R^2_m and R^2_c, respectively) values are provided. Based on the best-fitting linear mixed-effect models (Table S3), variance partitioning of the selected fixed- and random-effects variables, indicating the relative importance of each predictor, is also shown in Fig g, and the sample sizes are reported for each model. The variance inflation factor (vif) of each predictor variable in the linear mixed models is provided for all observations and subset modellings in table S4. MAT: The mean annual temperature at each site per year; Photoperiod: the length of time that an organism is exposed to sunlight each day, was calculated as the interval between

sunrise and sunset for each site; Chilling: the length of the period (days or hours) during which the temperature remains within the range of -5°C and 5°C, the reference period starting from November 1st of the previous year to the onset day of cell-wall-thickening; Forcing: the length of period (days or hours) during which the temperature remains above 5°C, the reference period starting from January 1st to the onset day of cell-wall-thickening; scPDSI: The self-calibrating Palmer Drought Severity Index, representing soil moisture (scPDSI ranging from -4 to 4, indicating from excessively dry to excessively moist); Tem_variation: the averaged standard deviation of the mean daily temperature in a 60-day period over the mean cell-wall-thickening DOY (60-day centered period) at each site and in the same year, this value was employed to represent the local spring temperature variance.

Discussion

Climate warming has resulted in a more uniform spring phenology between cold (high latitudes or altitudes) and warm (low latitudes or altitudes) ecosystems (Chen et al., 2018; Chen et al., 2019; Ma et al., 2018; Meng et al., 2020), suggesting a possible existence of a thermal threshold across ecosystems over a large spatial scale. Such a threshold may separate the biomes into regions with diverging advancing rates of tree spring phenology under global warming, i.e. a larger advancement at the higher latitudes or altitudes due to the benefit of warming *vs.* a smaller advancement at the lower latitudes or altitudes due to a higher forcing requirement induced by the reduced chilling accumulation. Our dataset showed evidence of an abrupt change in the advancement of cell-wall thickening of conifers along the gradient in mean annual temperature (MAT) over the Northern Hemisphere and corresponding with a threshold of 4.9±1.1℃ in MAT (Fig. 1a, b).

The air temperature, represented by MAT in our analyses, was the primary factor regulating the timings of cell-wall-thickening in cold ecosystems, whereas forcing was the main trigger in warm ecosystems. Our results suggest that global warming could continue to advance the onset in cell-wall thickening, but this advancement could slow down because of the increased requirement in forcing temperature in warm ecosystems. Our results provide empirical evidence for introducing a thermal transition into temperature-based models for a better understanding of temperature mechanisms and their geographical context. This inclusion will improve Earth System Models (ESMs) for predicting global forest phenology and productivity and biogeochemical cycles under climate warming.

A critical thermal transition revealed in the Northern Hemisphere

The abrupt change in the slopes of the advancement of the onset of cell-wall thickening at MAT of 4.9±1.1 ℃ (Fig. 1a) has important ecological implications, implying divergent advancing rates of forest phenology events could be quantitatively organized into a larger-smaller advancement spectrum: larger advancements in cold sites and smaller advancements in warm sites. The advancement of the onset of cell-wall thickening to rising temperatures would significantly slow down at a MAT of 4.9℃. Our research extends and advances prior research that the effects of climate warming on forest spring phenology are dependent on whether conditions (Gunderson et al., 2012; Montgomery et al., 2020). The greater advancement to rising temperature in cold ecosystems, associated with the reduction in advancement in the warm ecosystems, could reduce spatial variability. Therefore, we would expect a more uniform trend in spring phenology between cold and warm ecosystems under the ongoing warming conditions (Chen et al., 2019; Ettinger et al., 2020; Ma et al., 2018).

At the species level, early successional species showed a stronger advancing shift in cold sites than was observed for the late successional ones, and thus these two functional groups would shift further apart under rising temperatures. Hence, the cold sites would face fundamental changes in the timing of cell-wall thickening and the synchrony among tree species, with consequences for the plant communities and the whole ecosystem (Kharouba et al., 2018). However, the two successional groups showed a similar degree of shift in warm sites (Fig. 1b). Consequently, the early species exhibited a more substantial and abrupt decline in further advancement along the MAT gradient than did the late ones (Fig. 1b).

Drivers for cell-wall-thickening across the thermal threshold and underlying mechanisms

We explored key drivers of cell-wall-thickening DOY among six selected common potential predictors (MAT, photoperiod, forcing, chilling, scPDSI, and spring temperature variation, see Climate data and photoperiod in Supplementary Information Text for further details) using linear mixed effect models (LMMs) and

Bayesian mixed-effects models (BMMs). The main environmental drivers varied greatly for trees in the cold versus warm temperature regimes. MAT was the reason behind most of the variance in the timings of cell-wall-thickening in cold ecosystems, but its relative importance dropped in warm ecosystems (Fig. 2a, b, g). This confirmed that cell-wall-thickening in cold regions is strongly regulated by MAT. Therefore, the occurrence of the first xylem wall thickening cell becomes a matter of tracking the appropriate temperature across ecosystems and species (Begum et al., 2013; Rossi et al., 2016). Plants are submitted to a selective pressure to match their spring phenology to favorable environmental conditions and minimize the risk of frost (Mura et al., 2022), while at the same time maximizing the length of the growing season to ensure trees to safely complete secondary cell wall lignification before winter (Rossi et al., 2006). In cold and temperate climates, temperature is a limiting factor, and tracking global warming to obtain a long growing season and thus maximize annual carbon would become the priority of spring phenology.

In warmer ecosystems, the raise in temperature would reduce the accumulation of chilling (fig. S3b), which could decrease the advancement of forest spring phenology to rising temperature (Chen et al., 2019; Ma et al., 2018; Meng et al., 2020). The greater variance in the timings of cell-wall thickening explained by chilling in warm ecosystems demonstrates the possibility that the reduced chilling accumulation plays a role in reducing further advancement (Fu et al., 2015; Meng et al., 2020; Vitasse et al., 2018). However, the contribution of this factor was relatively small, suggesting that chilling was unable to explain completely the declining advancement of forest spring phenology, which is in line with previous studies (Ettinger et al., 2020; Fu et al., 2015). Instead, chilling exerted its influence mainly by improving the forcing requirement (Delpierre et al., 2019; Ma et al., 2018). Although increasing evidences ascribed the slowdown of the advancement of the onset of forest primary growth to a higher forcing temperature requirement induced by chilling insufficiency (Chen et al., 2019; Ma et al., 2018), it has only rarely been reported for the onset of xylem growth (Delpierre et al., 2019). Trees usually require exposure to a sufficient forcing temperature for the resumption of

xylem cell growth (Delpierre et al., 2019). The higher accumulation of forcing temperatures in warm ecosystems (fig. S3c) was thus expected to advance the onset of cell-wall thickening, but we observed declined advancing rate (Fig. 1). We raise the hypothesis that a decreasing chilling exposure in warm sites (fig. S3b) induced a higher forcing requirement (Chen et al., 2019; Delpierre et al., 2019; Ma et al., 2018). Forcing is the most important factor in determining the timings of cell-wall thickening in warm ecosystems (Fig. 2), which supported our hypothesis. A photoperiod limitation for further advancement was also captured in our study, as indicated by the greater variance explained by the photoperiod in warm ecosystems compared with cold ecosystems (Fig. 2) (Basler & Körner, 2012; Richardson et al., 2018; Zohner et al., 2016). The importance of the photoperiod was relatively low compared with forcing accumulation, in line with other studies showing that only a minor group (mainly from lower latitudes) of temperate trees were constrained by day length (Zohner et al., 2016 Rossi et al., 2015). Our results illustrated how the environmental factors interact in space and result in the divergent advancing rates of forest spring phenology described in the literature (Piao et al., 2019), and thus providing a new perspective for understanding the potential trajectories of forest growth dynamics under global changes.

Notably, MAT had a dominant influence for early successional species in cold sites (Fig. 2). This could be explained by the different life strategies, as they adopt more risky life strategy (Körner & Basler, 2010) and can better benefit from appropriate temperatures for cell-wall-thickening. By contrast, late successional species adopt more conservative strategies, are less responsive to rising temperatures, which reflects the process of natural selection in environments characterized by greater temperature fluctuations and higher frost frequency (fig. S8). There is evidence that early successional species are more likely to keep tracking climatic warming than late successional species (Basler & Körner, 2012; Fu et al., 2019; Körner & Basler, 2010). Moreover, once cross the transition, photoperiod and forcing temperatures had similar importance for early successional species.

To the best of our knowledge, this study is the first to provide a quantitative indication of the existence of a thermal threshold at MAT= 4.9±1.1℃, based on a

unique dataset describing the onset of cell-wall-thickening in Northern Hemisphere conifers. This thermal threshold classified all the studied sites into cold and warm ecosystems (Fig. 3a), where air temperature (represented by MAT) and forcing, respectively, were the primary drivers for triggering the onset of cell-wall thickening. Rising temperature will continue to advance the onset dates, but this advancement would significantly decline upon crossing the thermal transition toward warm ecosystems. For areas in current cold region (MAT < 4.9℃) that may turn into warm region predicted by climatic models (Fig. 3b), we would expect to see the advancing effects decline abruptly. The early and late successional species would be expected to shift further apart in cold ecosystems due to different advancing rates to rising temperatures. Conversely, in warm ecosystems, future global warming would exert less influence on the phenological synchrony of the early and late successional species due to their similar advancing rates. Our results clearly demonstrate how forest spring phenology will respond to rising temperature in two distinct phases, lending insights to the mechanisms behind the divergent results regarding phenological responses (Piao et al., 2019). The identified thermal threshold can be integrated into the Earth System Models to allow more accurate and reasonable prediction of global carbon, water and energy cycles under global warming (Montgomery et al., 2020; Wolkovich et al., 2012).

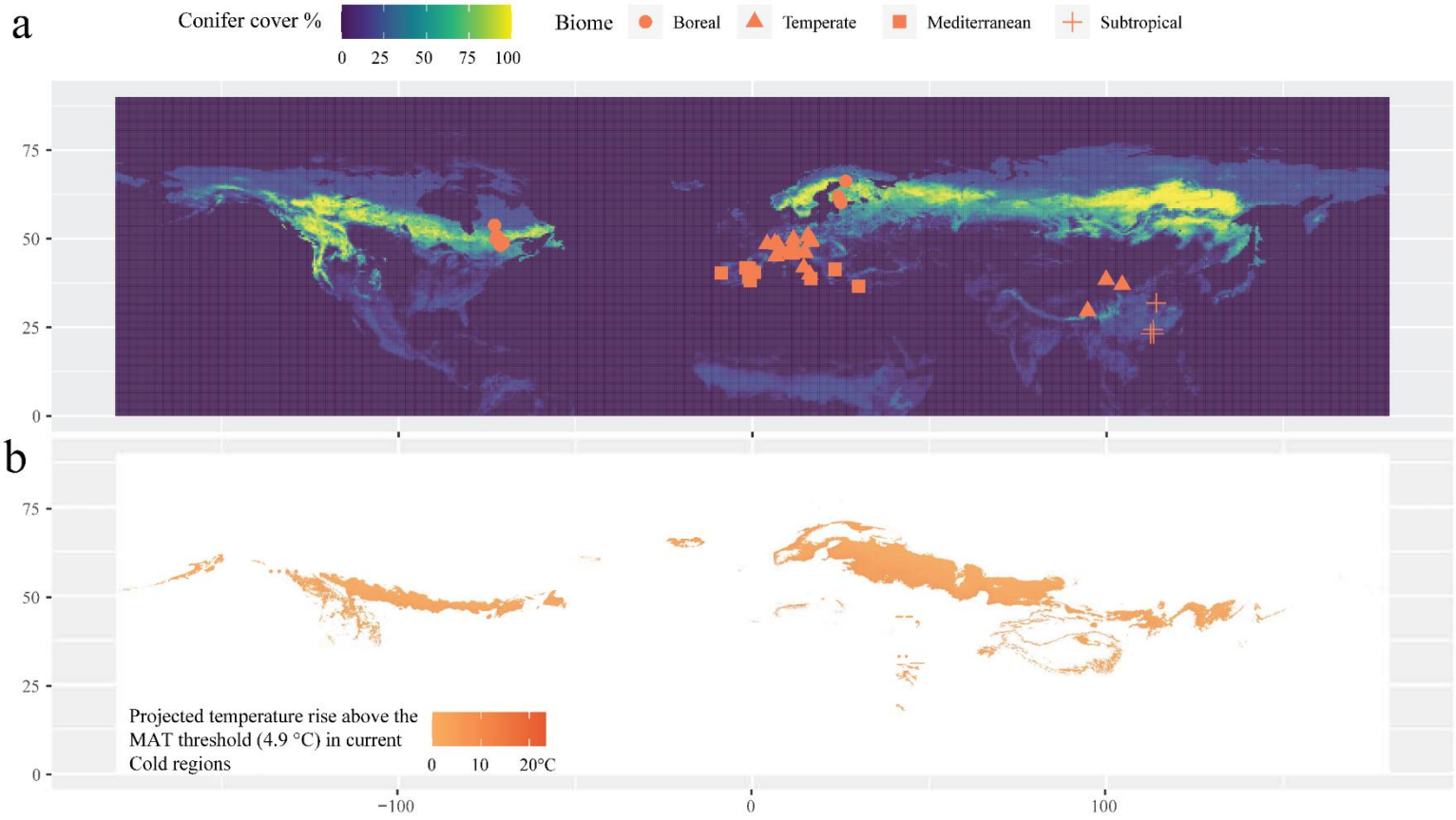

Fig 3. (a) Geographical distributions of global conifer cover (data from Global Forest Age Dataset (Poulter et al., 2019) and location of the study sites across the Northern Hemisphere. The numbers in the conifer cover legend denote the relative coniferous forest cover proportional to a specific total area in the Global Forest Age Dataset (GFAD) (Poulter et al., 2019). (b) Areas in current Cold region (MAT < 4.9℃) that may turn into Warm region in CMIP5 projected changes in MAT in the Northern hemisphere. This is predicted by the differences in MAT between the period of 1970-2000 (from worldclim.org) and the period of 2061-2080 (projected by CMIP5).

Acknowledgments

Funding: This work was funded by the Xinjiang Regional Collaborative Innovation Project (2022E01045) and the National Natural Science Foundation of China (32271653, 32001138), Zhejiang University (108000*1942222R1). Other funding agencies included the Austrian Science Fund (FWF P22280-B16; P25643-B16), Observatoire régional de recherche en forêt boréale, Consortium de Recherche sur la Forêt Boréale Commerciale, Fonds de Recherche sur la Nature et les Technologies du Québec, Forêt d'enseignement et de recherche Simoncouche, Natural Sciences and Engineering Research Council of Canada, Slovenian Research Agency ARRS (young researchers' program, programs P4-0015 and P4-0107, and project Z4-7318), MIUR-PRIN 2002 (2002075152) and 2005 (2005072877), Swiss National Science Foundation (Projects INTEGRAL-121859 and LOTFOR-150205), French National Research Agency (ANR) as part of the "Investissements d'Avenir" program (ANR-11-LABX-0002-01, Lab of Excellence ARBRE), Academy of Finland (Nos. 250299, 257641 and 265504), NSFC (41525001), Grant Agency of Czech Republic (P504/11/P557), and Provincia Autonoma di Trento (project "SOFIE 2" – 3012/2007). The cooperation among authors was supported by the EU COST Action FP1106 STReESS. The views and conclusions contained in this document are those of the authors and should not be interpreted as representing the opinions or policies of the funding agencies and supporting institutions.

Author Contributions:

JH, YL and YZ designed this study. YZ, MW, and XY analyzed the data. JH and YZ wrote the manuscript with assistance from SR and YL. All coauthors contributed to this work in various ways including conducting field experiments, laboratory work, pre-processing, and contribution of data, as well as by commenting on and improving the manuscript.

References:

Abe, H., Funada, R., Ohtani, J., & Fukazawa, K. (1997). Changes in the arrangement of cellulose microfibrils associated with the cessation of cell expansion in tracheids. *Trees, 11*(6), 328-332.

Antonucci, S., Rossi, S., Deslauriers, A., Lombardi, F., Marchetti, M., & Tognetti, R. (2015). Synchronisms and correlations of spring phenology between apical and lateral meristems in two boreal conifers. *Tree Physiology, 35*(10), 1086-1094.

Asse, D., Chuine, I., Vitasse, Y., Yoccoz, N. G., Delpierre, N., Badeau, V., . . . Randin, C. F. (2018). Warmer winters reduce the advance of tree spring phenology induced by warmer springs in the Alps. *Agricultural and Forest Meteorology, 252*, 220-230.

Basler, D., & Körner, C. (2012). Photoperiod sensitivity of bud burst in 14 temperate forest tree species. *Agricultural and Forest Meteorology, 165*, 73-81.

Begum, S., Kudo, K., Rahman, M. H., Nakaba, S., Yamagishi, Y., Nabeshima, E., . . . Jin, H.-O. (2018). Climate change and the regulation of wood formation in trees by temperature. *Trees, 32*(1), 3-15.

Begum, S., Nakaba, S., Yamagishi, Y., Oribe, Y., & Funada, R. (2013). Regulation of cambial activity in relation to environmental conditions: understanding the role of temperature in wood formation of trees. *Physiologia Plantarum, 147*(1), 46-54.

Berdugo, M., Delgado-Baquerizo, M., Soliveres, S., Hernández-Clemente, R., Zhao, Y., Gaitán, J. J., . . . Lehmann, A. (2020). Global ecosystem thresholds driven by aridity. *Science, 367*(6479), 787-790.

Burnham, K. P., Anderson, D. R., & Huyvaert, K. P. (2011). AIC model selection and multimodel inference in behavioral ecology: some background, observations, and comparisons. *Behavioral ecology and sociobiology, 65*(1), 23-35.

Caffarra, A., & Donnelly, A. (2011). The ecological significance of phenology in four different tree species: effects of light and temperature on bud burst. *International journal of Biometeorology, 55*(5), 711-721.

Chen, L., Huang, J. G., Ma, Q., Hänninen, H., Rossi, S., Piao, S., & Bergeron, Y. (2018). Spring phenology at different altitudes is becoming more uniform under global warming in Europe. *Global Change Biology, 24*(9), 3969-3975.

Chen, L., Huang, J. G., Ma, Q., Hänninen, H., Tremblay, F., & Bergeron, Y. (2019). Long‐term changes in the impacts of global warming on leaf phenology of four temperate tree species. *Global Change Biology, 25*(3), 997-1004.

Cuny, H. E., Rathgeber, C. B., Frank, D., Fonti, P., Mäkinen, H., Prislan, P., . . . Vavrčík, H. (2015). Woody biomass production lags stem-girth increase by over one month in coniferous forests. *Nature Plants, 1*(11), 1-6.

Delpierre, N., Lireux, S., Hartig, F., Camarero, J. J., Cheaib, A., Čufar, K., . . . Gričar, J. (2019). Chilling and forcing temperatures interact to predict the onset of wood formation in Northern Hemisphere conifers. *Global Change Biology, 25*(3), 1089-1105.

Delpierre, N., Vitasse, Y., Chuine, I., Guillemot, J., Bazot, S., & Rathgeber, C. B. (2016). Temperate and boreal forest tree phenology: from organ-scale processes to terrestrial ecosystem models. *Annals of Forest Science, 73*(1), 5-25.

Deslauriers, A., Morin, H., & Begin, Y. (2003). Cellular phenology of annual ring formation of Abies balsamea in the Quebec boreal forest (Canada). *Canadian Journal of Forest Research, 33*(2), 190-200.

Elith, J., Leathwick, J. R., & Hastie, T. (2008). A working guide to boosted regression trees. *Journal of Animal Ecology, 77*(4), 802-813.

Elmendorf, S. C., Henry, G. H., Hollister, R. D., Fosaa, A. M., Gould, W. A., Hermanutz, L., . . . Lévesque, E. (2015). Experiment, monitoring, and gradient methods used to infer climate change effects on plant communities yield consistent patterns. *Proceedings of the National Academy of Sciences, 112*(2), 448-452.

Ettinger, A., Chamberlain, C., Morales-Castilla, I., Buonaiuto, D., Flynn, D., Savas, T., . . . Wolkovich, E. (2020). Winter temperatures predominate in spring phenological responses to warming. *Nature Climate Change, 10*(12), 1137-1142.

Fox, J., & Weisberg, S. (2018). *An R companion to applied regression*: Sage publications.

Frey, S. J., Hadley, A. S., Johnson, S. L., Schulze, M., Jones, J. A., & Betts, M. G. (2016). Spatial models reveal the microclimatic buffering capacity of old-growth forests. *Science advances, 2*(4), e1501392.

Fu, Y. H., Piao, S., Zhou, X., Geng, X., Hao, F., Vitasse, Y., & Janssens, I. A. (2019). Short photoperiod reduces the temperature sensitivity of leaf‐out in saplings of Fagus sylvatica but not in horse chestnut. *Global Change Biology, 25*(5), 1696-1703.

Fu, Y. H., Zhao, H., Piao, S., Peaucelle, M., Peng, S., Zhou, G., . . . Peñuelas, J. (2015). Declining global warming effects on the phenology of spring leaf unfolding. *Nature, 526*(7571), 104-107.

Gunderson, C. A., Edwards, N. T., Walker, A. V., O'Hara, K. H., Campion, C. M., & Hanson, P. J. (2012). Forest phenology and a warmer climate–growing season extension in relation to climatic provenance. *Global Change Biology, 18*(6), 2008-2025.

Hastie, T. J. (2017). Generalized additive models. In *Statistical models in S* (pp. 249-307): Routledge.

Hoffman, G. E., & Schadt, E. E. (2016). variancePartition: interpreting drivers of variation in complex gene expression studies. *BMC bioinformatics, 17*(1), 1-13.

Huang, J.-G., Ma, Q., Rossi, S., Biondi, F., Deslauriers, A., Fonti, P., & Liang, E. (2020). Photoperiod and temperature as dominant environmental drivers triggering secondary growth resumption in Northern Hemisphere conifers. *Proceedings of the National Academy of Sciences, 117*(34), 20645-20652.

Kharouba, H. M., Ehrlén, J., Gelman, A., Bolmgren, K., Allen, J. M., Travers, S. E., & Wolkovich, E. M. (2018). Global shifts in the phenological synchrony of species interactions over recent decades. *Proceedings of the National Academy of Sciences, 115*(20), 5211-5216.

Körner, C., & Basler, D. (2010). Phenology under global warming. *Science, 327*(5972), 1461-1462.

Kuznetsova, A., Brockhoff, P. B., & Christensen, R. H. B. (2014). lmerTest: Tests for random and fixed effects for linear mixed effect models. R package version 2.0-11. *URL http://CRAN. R-project. org/package= lmerTest*.

Logan, M. L., Cox, R. M., & Calsbeek, R. (2014). Natural selection on thermal performance in a novel thermal environment. *Proceedings of the National Academy of Sciences, 111*(39), 14165-14169.

Ma, Q., Huang, J.-G., Hänninen, H., & Berninger, F. (2018). Reduced geographical variability in spring phenology of temperate trees with recent warming. *Agricultural and Forest Meteorology, 256*, 526-533.

McClanahan, T. R., Darling, E. S., Maina, J. M., Muthiga, N. A., D'agata, S., Jupiter, S. D., . . . Nand, Y. (2019). Temperature patterns and mechanisms influencing coral bleaching during the 2016 El Niño. *Nature Climate Change, 9*(11), 845-851.

Meng, L., Mao, J., Zhou, Y., Richardson, A. D., Lee, X., Thornton, P. E., . . . Shi, X. (2020). Urban warming advances spring phenology but reduces the response of phenology to temperature in the conterminous United States. *Proceedings of the National Academy of Sciences, 117*(8), 4228-4233.

Menzel, A., Sparks, T. H., Estrella, N., Koch, E., Aasa, A., Ahas, R., . . . Briede, A. (2006). European phenological response to climate change matches the warming pattern. *Global Change Biology, 12*(10), 1969-1976.

Montgomery, R. A., Rice, K. E., Stefanski, A., Rich, R. L., & Reich, P. B. (2020). Phenological responses of temperate and boreal trees to warming depend on ambient spring temperatures, leaf habit, and geographic range. *Proceedings of the National Academy of Sciences, 117*(19), 10397-10405.

Moser, L., Fonti, P., Büntgen, U., Esper, J., Luterbacher, J., Franzen, J., & Frank, D. (2010). Timing and duration of European larch growing season along altitudinal gradients in the Swiss Alps. *Tree Physiology, 30*(2), 225-233.

Muggeo, V. M. (2008). Segmented: an R package to fit regression models with broken-line relationships. *R news, 8*(1), 20-25.

Mura C, Buttò V, Silvestro R, Deslauriers A, Charrier G, Raymond P, Rossi S. The early bud gets the cold: diverging spring phenology drives exposure to late frost in a *Picea mariana* [(Mill.) BSP] common garden. *Physiologia Plantarum*, in press

Oribe, Y., Funada, R., & Kubo, T. (2003). Relationships between cambial activity, cell differentiation and the localization of starch in storage tissues around the cambium in locally heated stems of Abies sachalinensis (Schmidt) Masters. *Trees, 17*(3), 185-192.

Ortiz-Bobea, A., Knippenberg, E., & Chambers, R. G. (2018). Growing climatic sensitivity of US agriculture linked to technological change and regional specialization. *Science advances, 4*(12), eaat4343.

Peters, M. K., Hemp, A., Appelhans, T., Becker, J. N., Behler, C., Classen, A., . . . Frederiksen, S. B. (2019). Climate–land-use interactions shape tropical mountain biodiversity and ecosystem functions. *Nature, 568*(7750), 88-92.

Piao, S., Liu, Q., Chen, A., Janssens, I. A., Fu, Y., Dai, J., . . . Zhu, X. (2019). Plant phenology and global climate change: Current progresses and challenges. *Global Change Biology, 25*(6), 1922-1940.

Poulter, B., Aragão, L., Andela, N., Bellassen, V., Ciais, P., Kato, T., ... & Shivdenko, A. (2019). The global forest age dataset and its uncertainties (GFADv1. 1).

Prevéy, J., Vellend, M., Rüger, N., Hollister, R. D., Bjorkman, A. D., Myers‐Smith, I. H., . . . Elberling, B. (2017). Greater temperature sensitivity of plant phenology at colder sites: implications for convergence across northern latitudes. *Global Change Biology, 23*(7), 2660-2671.

Richardson, A. D., Hufkens, K., Milliman, T., Aubrecht, D. M., Furze, M. E., Seyednasrollah, B., . . . Heiderman, R. R. (2018). Ecosystem warming extends vegetation activity but heightens vulnerability to cold temperatures. *Nature, 560*(7718), 368-371.

Richardson, A. D., Keenan, T. F., Migliavacca, M., Ryu, Y., Sonnentag, O., & Toomey, M. (2013). Climate change, phenology, and phenological control of vegetation feedbacks to the climate system. *Agricultural and Forest Meteorology, 169*, 156-173.

Rossi, S. (2015). Local adaptations and climate change: converging sensitivity of bud break in black spruce provenances. *International Journal of Biometeorology*, 59(7), 827-835.

Rossi, S., Anfodillo, T., Čufar, K., Cuny, H. E., Deslauriers, A., Fonti, P., . . . Huang, J. G. (2016). Pattern of xylem phenology in conifers of cold ecosystems at the Northern Hemisphere. *Global Change Biology*, *22*(11), 3804-3813.

Rossi, S., Deslauriers, A., Anfodillo, T., Morin, H., Saracino, A., Motta, R., & Borghetti, M. (2006). Conifers in cold environments synchronize maximum growth rate of tree‐ring formation with day length. *New Phytologist, 170*(2), 301-310.

Venter, Z., Cramer, M., & Hawkins, H.-J. (2018). Drivers of woody plant encroachment over Africa. *Nature communications, 9*(1), 1-7.

Vitasse, Y., Lenz, A., & Körner, C. (2014). The interaction between freezing tolerance and phenology in temperate deciduous trees. *Frontiers in Plant Science*, *5*(541). doi:10.3389/fpls.2014.00541

Vitasse, Y., Signarbieux, C., & Fu, Y. H. (2018). Global warming leads to more uniform spring phenology across elevations. *Proceedings of the National Academy of Sciences, 115*(5), 1004-1008.

Warton, D. I., Duursma, R. A., Falster, D. S., & Taskinen, S. (2012). smatr 3–an R package for estimation and inference about allometric lines. *Methods in Ecology and Evolution*, *3*(2), 257-259.

Wolkovich, E. M., Cook, B. I., Allen, J. M., Crimmins, T. M., Betancourt, J. L., Travers, S. E., . . . Kraft, N. J. (2012). Warming experiments underpredict plant phenological responses to climate change. *Nature, 485*(7399), 494-497.

Zohner, C. M., Benito, B. M., Svenning, J.-C., & Renner, S. S. (2016). Day length unlikely to constrain climate-driven shifts in leaf-out times of northern woody plants. *Nature Climate Change, 6*(12), 1120-1123.

Supplementary Materials for

A critical thermal transition driving spring phenology of Northern Hemisphere conifers

Jian-Guo Huang[*], Yaling Zhang[*], Minhuang Wang, Xiaohan Yu, Annie Deslauriers, Patrick Fonti, Eryuan Liang, Harri Mäkinen, Walter Oberhuber, Cyrille B. K. Rathgeber, Roberto Tognetti, Václav Treml, Bao Yang, Lihong Zhai, Jiao-Lin Zhang, Serena Antonucci, Yves Bergeron, J. Julio Camarero, Filipe Campelo, Katarina Čufar, Henri E. Cuny, Martin De Luis, Marek Fajstavr, Alessio Giovannelli, Jožica Gričar, Andreas Gruber, Vladimír Gryc, Aylin Güney Tuula Jyske, Jakub Kašpar, Gregory King, Cornelia Krause, Audrey Lemay, Feng Liu, Fabio Lombardi, Edurne Martinez del Castillo, Hubert Morin, Cristina Nabais, Pekka Nöjd, Richard L. Peters, Peter Prislan, Antonio Saracino, Vladimir V. Shishov, Irene Swidrak, Hanuš Vavrčík, Joana Vieira, Qiao Zeng, Yu Liu[‡], and Sergio Rossi

[*] These authors contributed equally to this work.

[‡] To whom correspondence may be addressed.

Corresponding author: Yu Liu

Key Lab of Guangdong for Utilization of Remote Sensing and Geographical Information System, Guangdong Open Laboratory of Geospatial Information Technology and Application, Guangzhou Institute of Geography, Guangzhou 510070, China

Email: liuyu@loess.llqg.ac.cn

Materials and Methods

Climate data and photoperiod

A meteorological station was installed in a forest gap beside or close to the sampled trees at most sites. For the remaining sites, data from the nearest meteorological stations were downloaded from NOAA (https://www.ncdc.noaa.gov/cdo-web/datatools/findstation) (table S1). Temperature and precipitation were derived from sensors fixed at 2–3 m above the ground. Temperature was measured every 15 min and stored in dataloggers as hourly averages. From the recorded data, the minimum, mean, and maximum daily temperatures were calculated for further analyses. Occasionally, a few missing or abnormal daily values were estimated from the nearby weather stations from NOAA. The mean annual temperature (MAT) represents one common and meaningful variable for describing the xylem dynamics over the Northern Hemisphere (Gričar, Čufar, Oven, & Schmitt, 2005). MAT was then computed to represent the local climate of the sites in the studied regions, from boreal to subtropical biomes, and the thermal conditions occurring during the cell wall thickening (Gričar et al., 2005). The self-calibrating Palmer Drought Severity Index (scPDSI), representing soil moisture (scPDSI ranging from -4 to 4, indicating from excessively dry to excessively moist), has been confirmed to drive the onset of xylem formation in Northern Hemisphere conifers (Huang et al., 2020). The value taken the month before the onset had the best performance in model building when compared to the scPDSI obtained from other months, including January to June or combinations over multiple months (Huang et al., 2020). We obtained scPDSI data in the month before the beginning of cell-wall thickening with a spatial resolution of 0.5°from CRU scPDSI 4.03 (Rossi et al., 2016). Photoperiod, i.e. the day length, was calculated as the interval between sunrise and sunset for each site using the R package “insol” (http://www.meteoexploration.com/R/insol/).

Chilling and Forcing

The chilling requirement is normally defined as the length of the period (days or hours) during

which the temperature remains within a specific range (Fu et al., 2015). The forcing requirement is defined as the length of period (days or hours) during which the temperature remains above a specific range (Cleland et al., 2007). Previous studies have reported that a temperature range between -5°C and 5°C, for the reference period starting from November 1st of the previous year to the onset day of cambium activity, is the most effective for a chilling unit calculation (Huang et al., 2020). By contrast, the temperature threshold above 5°C, for the period starting from January 1st to the onset day of cambium activity, is most effective for the forcing unit calculation (Huang et al., 2020). We summed the number of days when the daily temperature was within this range and above the threshold of 5°C following the same abovementioned reference period for the calculation of both the chilling and the forcing requirements for the appearance of the first wall-thickening cell.

Forcing was computed using a sigmoid function of the average daily air temperature (Hänninen, 1990) as follow:

$$FU = \sum_{t_0}^{t_d} D_{FU} \qquad if\ T_t > T_{th} \qquad where\ \ D_{FU} = \frac{28.4}{1+e^{-0.185(T_t-18.4)}}$$

where FU is the spring forcing unit for the cell-wall-thickening DOY, D_{FU} is the daily forcing unit, t_0 is the start date for forcing accumulation (here assumed to be January 1st), t_d is the date of appearance of the first wall-thickening cell, T_t is the mean daily air temperature, and T_{th} is the threshold temperature above 5°C for forcing accumulation (Huang et al., 2020). To avoid misleading, it should be noted that there are up to eight models to calculate the spring forcing unit (but see Wang et al. 2020), and it should be cautious that the maximum temperature (28.4°C) defined here may not be universal for all study sites. For example, the FU in subtropical areas (red dots in Fig. S4c) may be marginally underestimated; nonetheless, given limited sampling points in these areas and a plateau phase of cell-wall-thickening onset documented at the high FU (Fig. S2b), major findings from the overall analyses are verified to be solid.

Local spring temperature variance and frost frequency

In cold climates, plants are exposed to large seasonal fluctuations in temperature. For example, temperatures in the boreal region could range from +25 to -50 °C during the course of the year (Murray et al., 1989), so simply tracking warming temperatures at the "wrong" time of the year would lead potentially to frost damage. Trees in these regions have evolved to be less responsive to rising temperature; consequently, the advancement of spring phenology declines with increased variance in local spring temperature (Way & Montgomery, 2015). Therefore, we modified a previous method (Wang et al., 2014) to calculate the local spring temperature variance and frost frequency. Specifically, at each site and year, we centered the averaged standard deviation (SD) of the mean daily temperature in a 60-day period over the mean cell-wall-thickening DOY (60-day centered period), and we used this as the spring SD. Thereafter, this value was employed to represent the local spring temperature variance (hereafter referred as Tem_variation). The number of frost days, which are defined as days with daily minimum temperatures <0°C over the 60-day centered period, was determined for each year. Spring frost frequency was then calculated by dividing the mean number of frost days by the length of the 60-day centered period (Frey et al., 2016).

Figures S1-S9

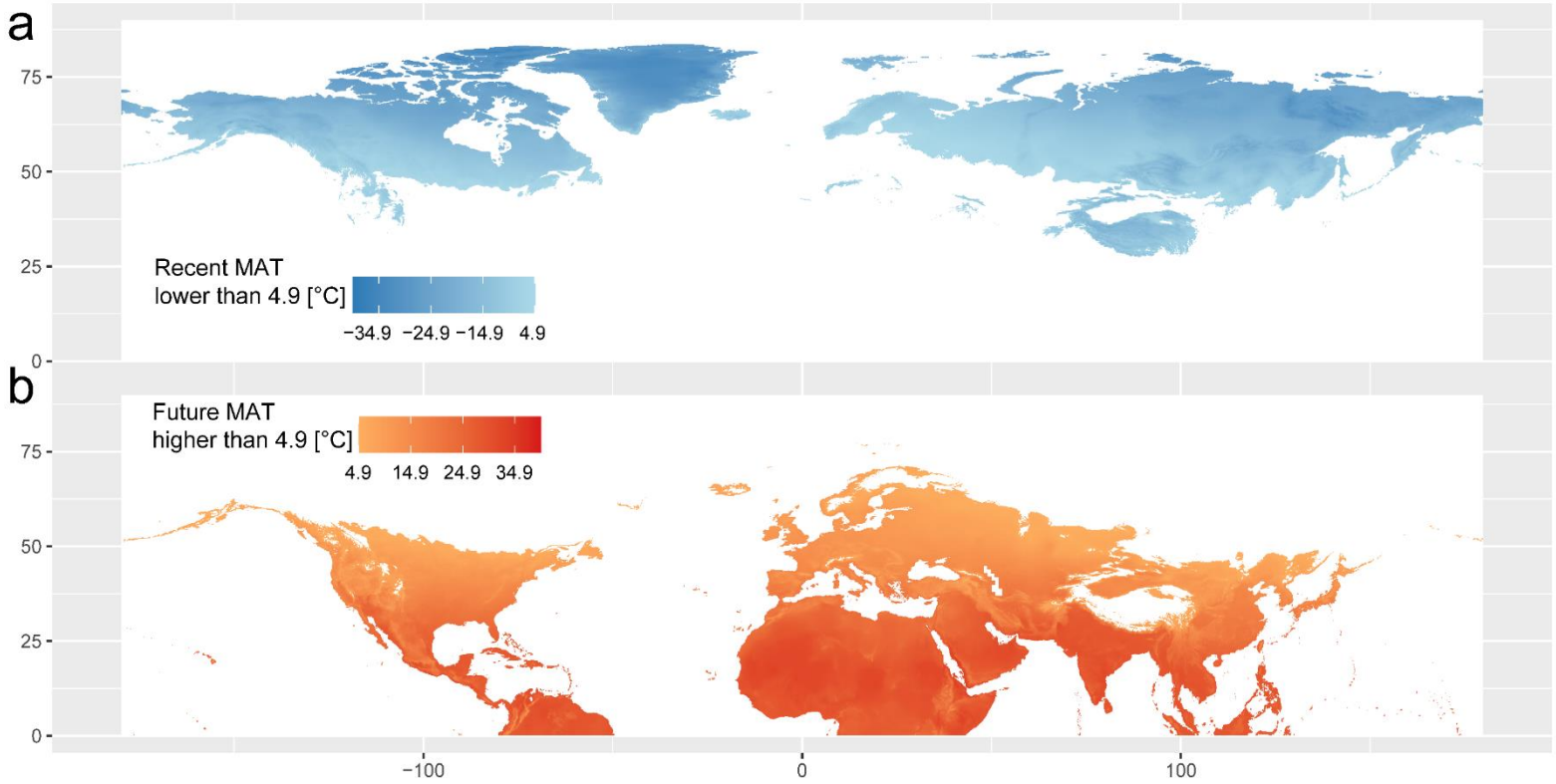

Fig. S1: (a) Northern Hemisphere regions with mean annual temperature (MAT) ＜4.9℃ during the period of 1970-2000 (data from worldclim.org) and (b) Northern Hemisphere regions with CMIP5 projected MAT ＞4.9℃ during the period of 2061-2080.

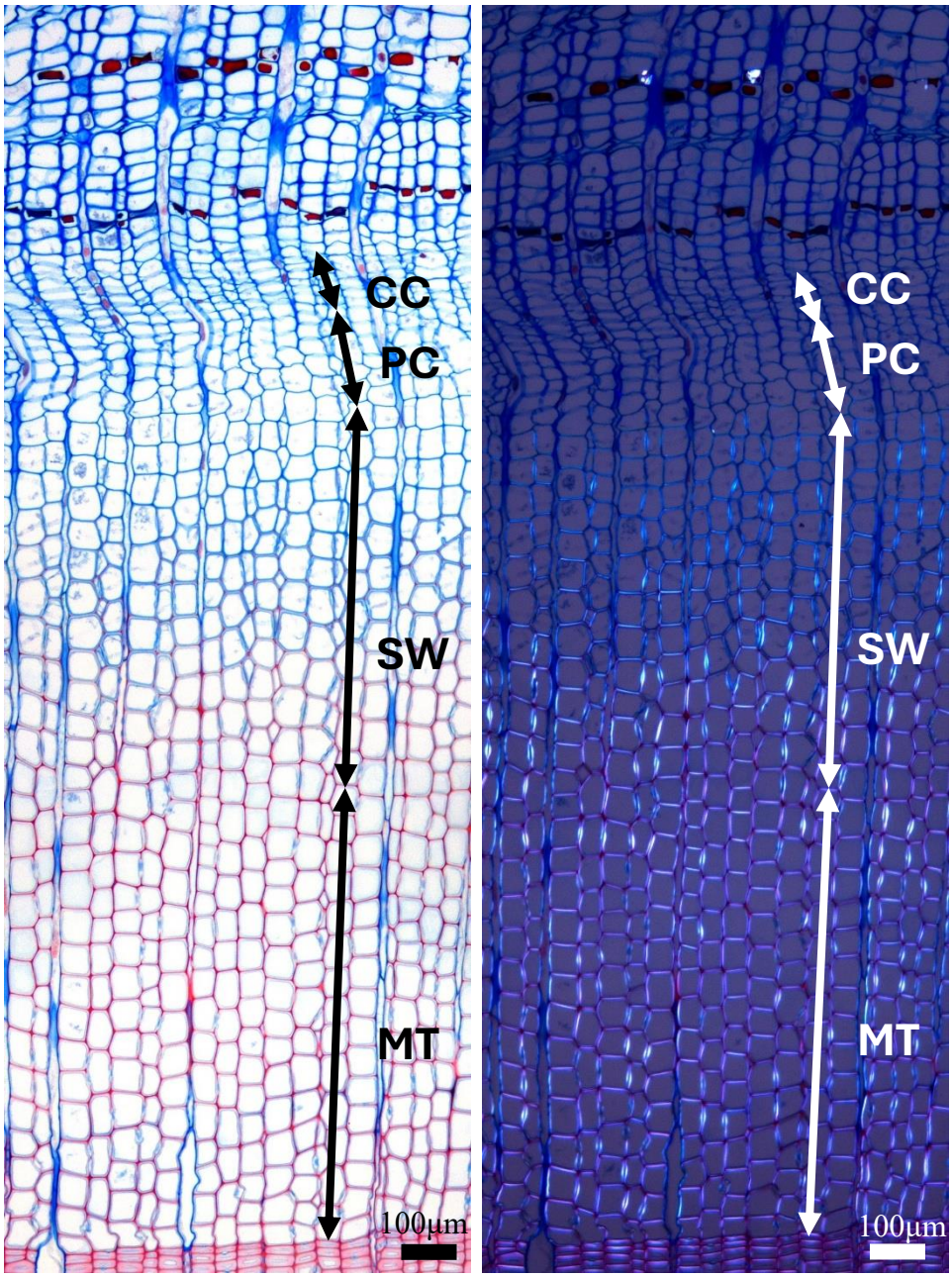

Fig. S2: Xylem growth rings of Norway spruce (*Picea abies*) in the middle of the growing season showing tracheids at different differentiation stages. Just below the cambium (CC) are cells in the enlargement stage (PC), followed by cells in the phase of secondary wall formation and wall-thickening (SW), and then mature cells (MT).

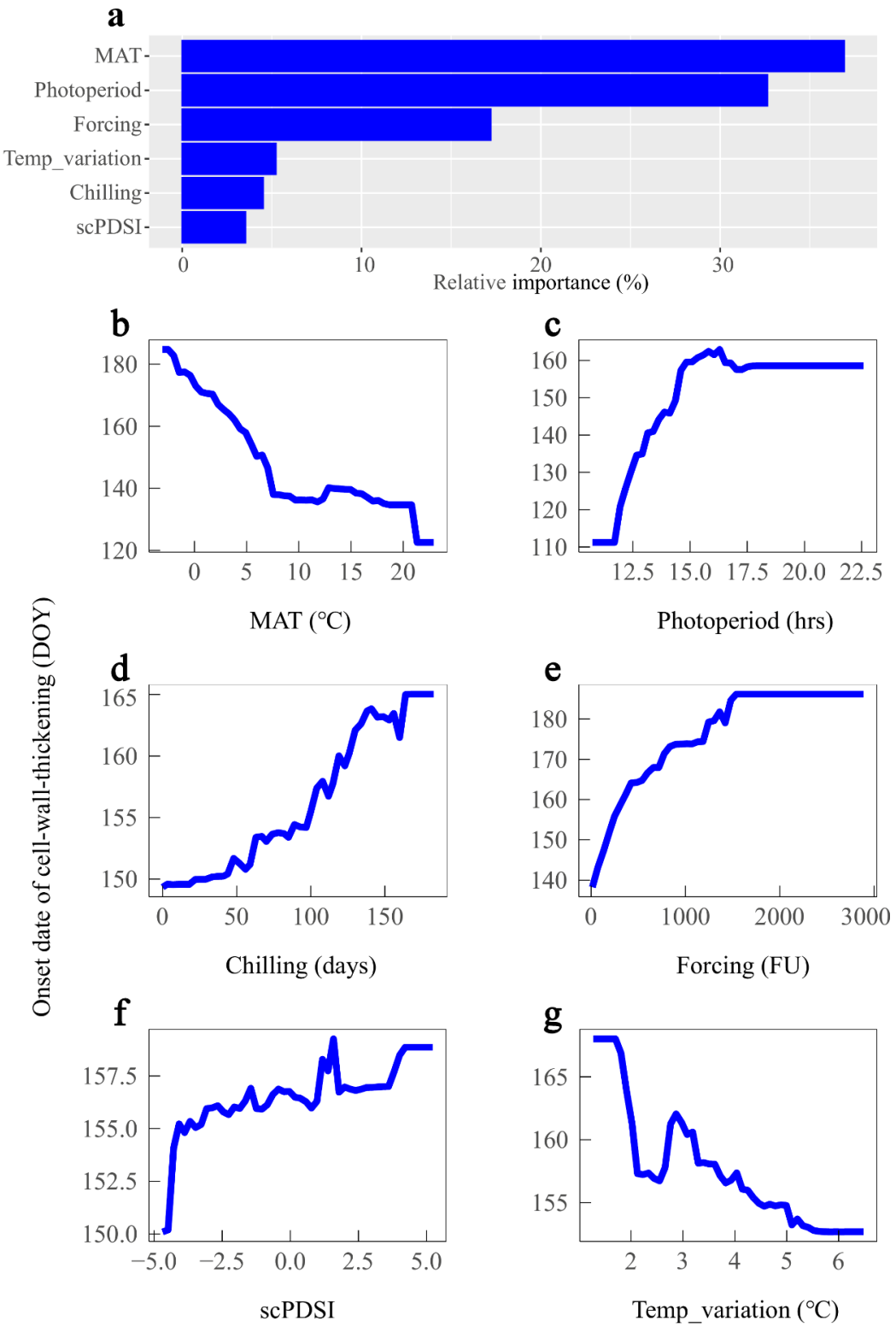

Figure S3. Variable importance from the boosted regression tree (a) showing the marginal effect of the predictor on the cell-wall-thickening DOY probability. These predictors were ranked by their relative importance; (b-g) Partial dependence plots of cell-wall-thickening DOY (day of the year) on mean annual temperature (MAT), photoperiod, chilling, forcing, scPDSI, and spring temperature variation (Temp_variation).

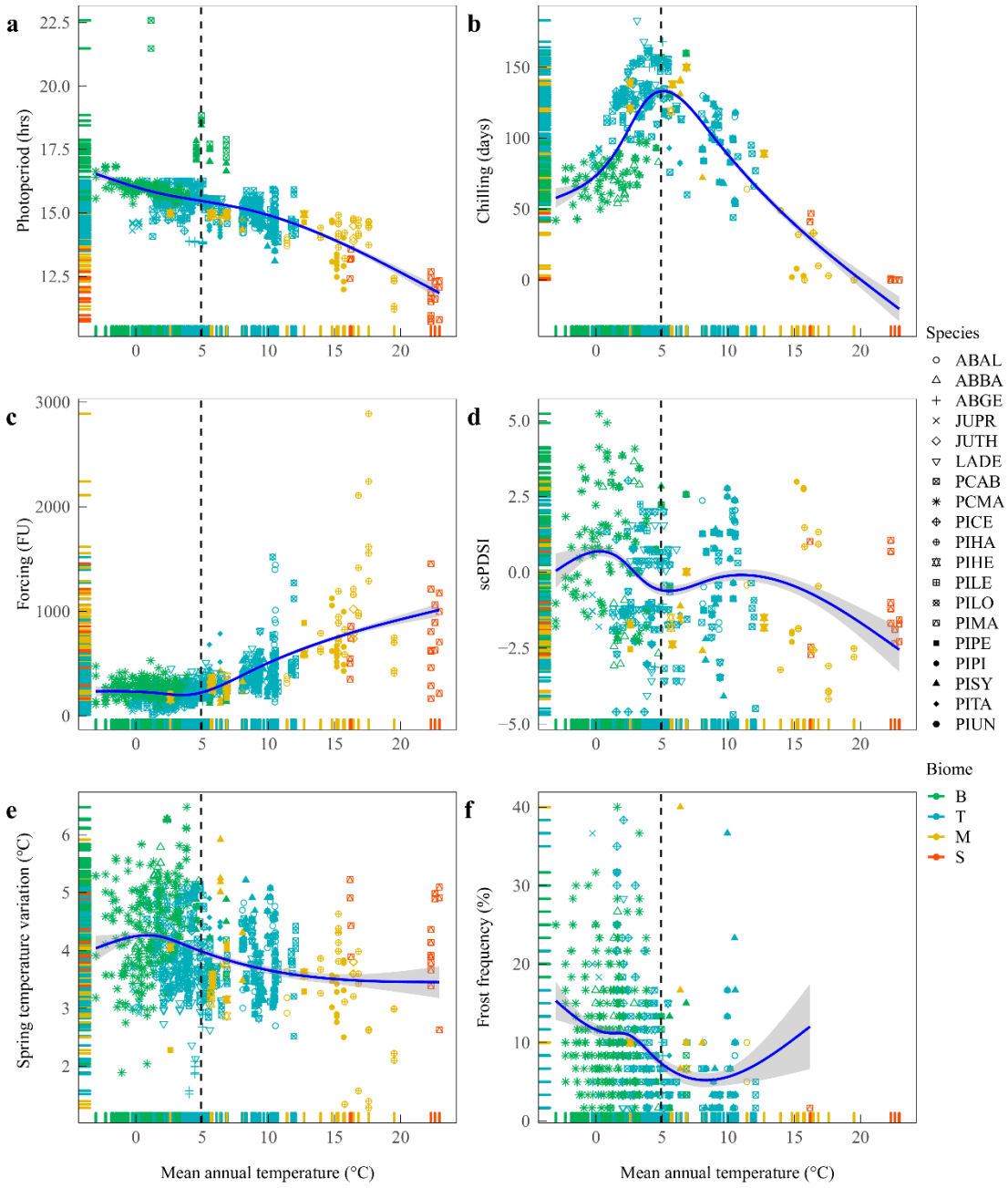

Figure S4: Variation in photoperiod (a), chilling (b), forcing (c), scPDSI (d), spring temperature variance (e), and frost frequency (f), according to the mean annual temperature (MAT) at the sites. Regression lines represent the predicted values estimated by natural cubic splines. Shadowed areas indicate 95% confidence interval. Biomes include boreal (B), temperate (T), Mediterranean (M), and subtropical (S).

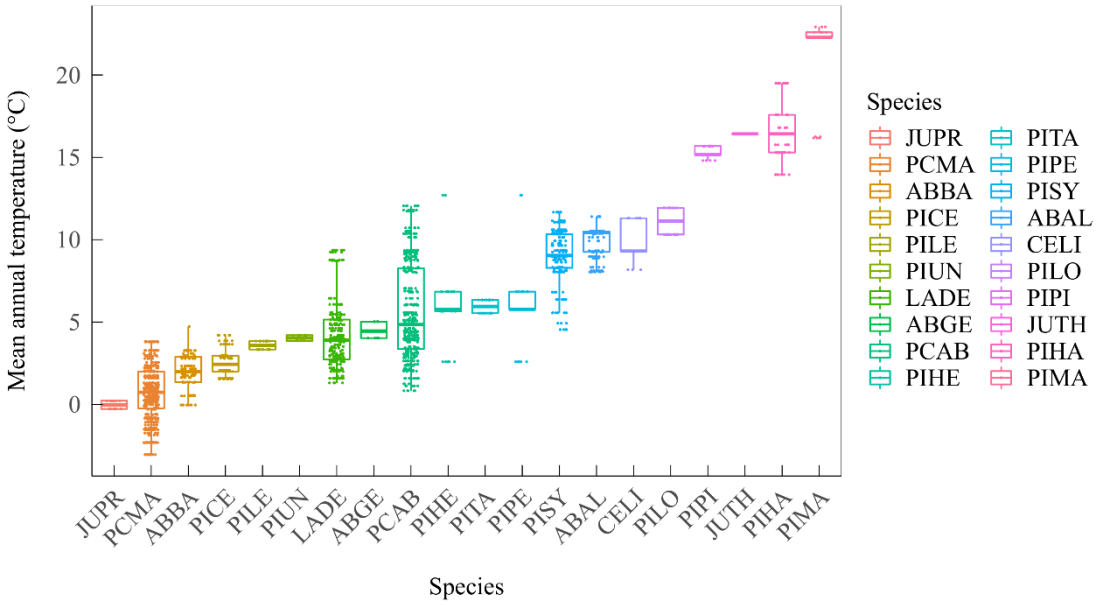

Figure S5: Boxplots, with jitter, displaying the distribution of selected tree species ranging across the mean annual temperature (MAT) gradients. Species are reported with the following acronyms and classified into early (JUPR, *Juniperus przewalskii*; JUTH, *Juniperus thurifera*; LADE, *Larix decidua*; PIHA, *Pinus halepensis*,; PIHE, *Pinus heldreichii*; PILE, *Pinus leucodermis*; PILO, *Pinus longaeva*; PIMA, *Pinus massoniana*; PIPE, *Pinus peuce*; PIPI, *Pinus pinaster*; PISY, *Pinus sylvestris*; PITA, *Pinus tabulaeformis*; and PIUN, *Pinus uncina*) and late (ABAL, *Abies alba*; ABBA, *Abies balsamea*; ABGE, *Abies georgei*; CELI, *Cedrus libani*; PCAB, *Picea abies*; PCMA, *Picea mariana*; PICE, *Pinus cembra*) successional species types (see Species classification Materials and Methods).

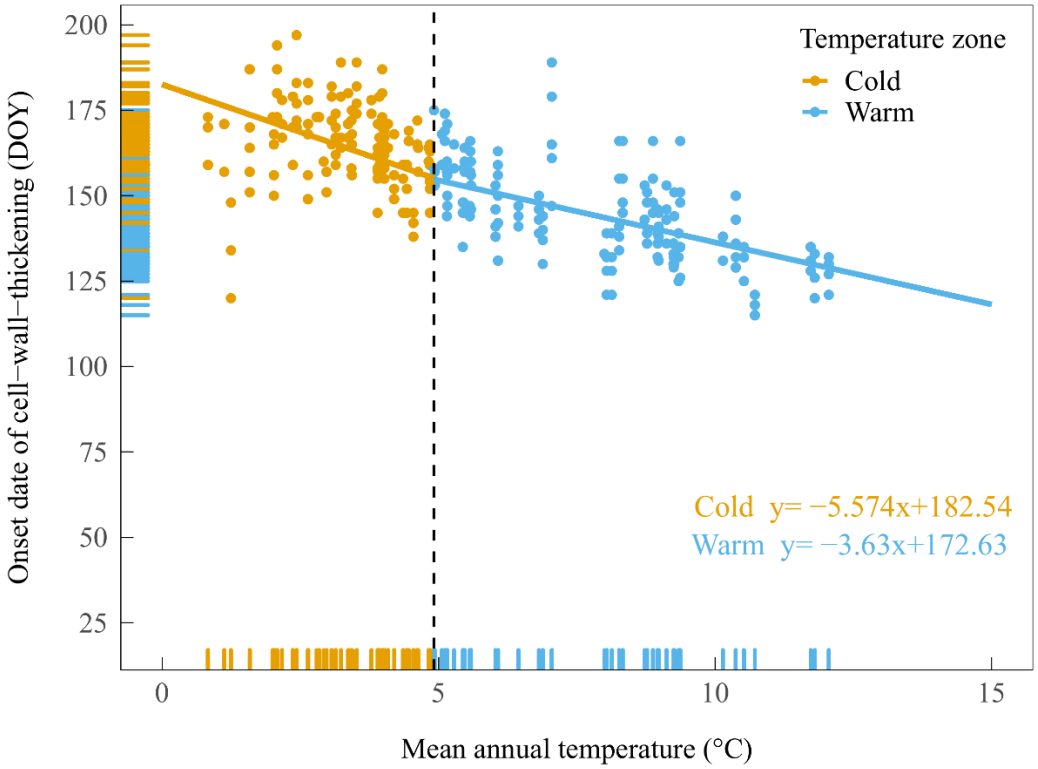

Figure S6: Changes in the cell-wall-thickening DOY (day of the year) for *Picea abies* (PCAB) along the mean annual temperature (MAT) gradients of sites, as fitted by a linear mixed effect model with sites as the random effect.

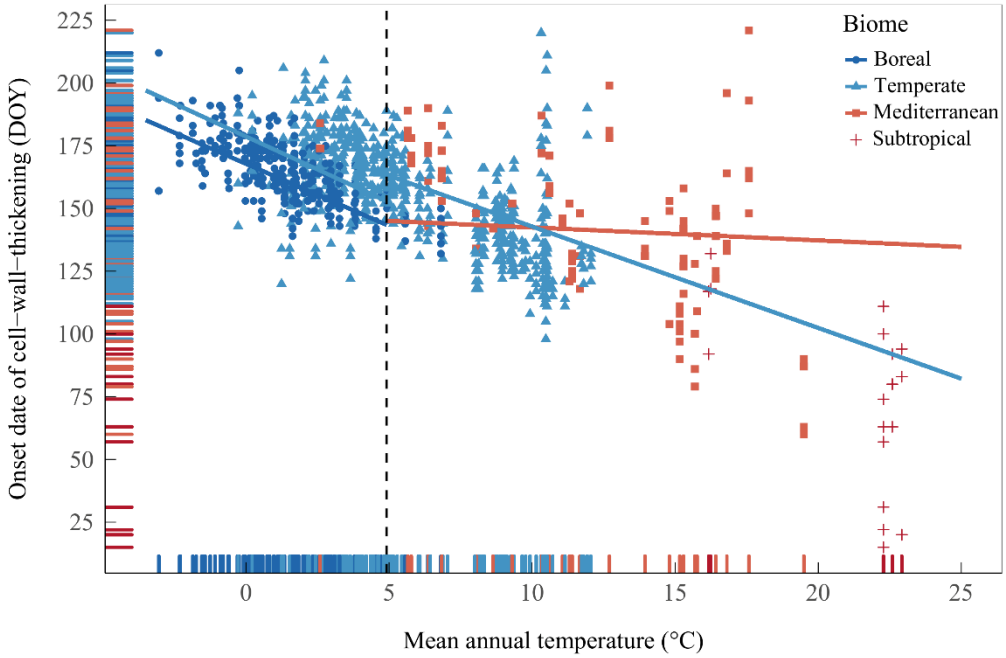

Figure S7: Changes in cell-wall-thickening DOY (day of the year) along the mean annual temperature (MAT) gradients of the sites (a) between the cold and warm sites classified by the

transition temperature at MAT=4.9±1.1℃ across biomes: boreal sites excluded the few dots above 4.9 ℃ (intercept: 167.86, slope: -4.96), cold-temperate sites (MAT below 4.9 ℃; intercept: 178.68, slope: -5.24), warm-temperate sites (MAT above 4.9 ℃; intercept: 183.22, slope: -4.04); Mediterranean sites excluded the few dots below 4.9 ℃ (intercept: 147.60, slope: -0.515).

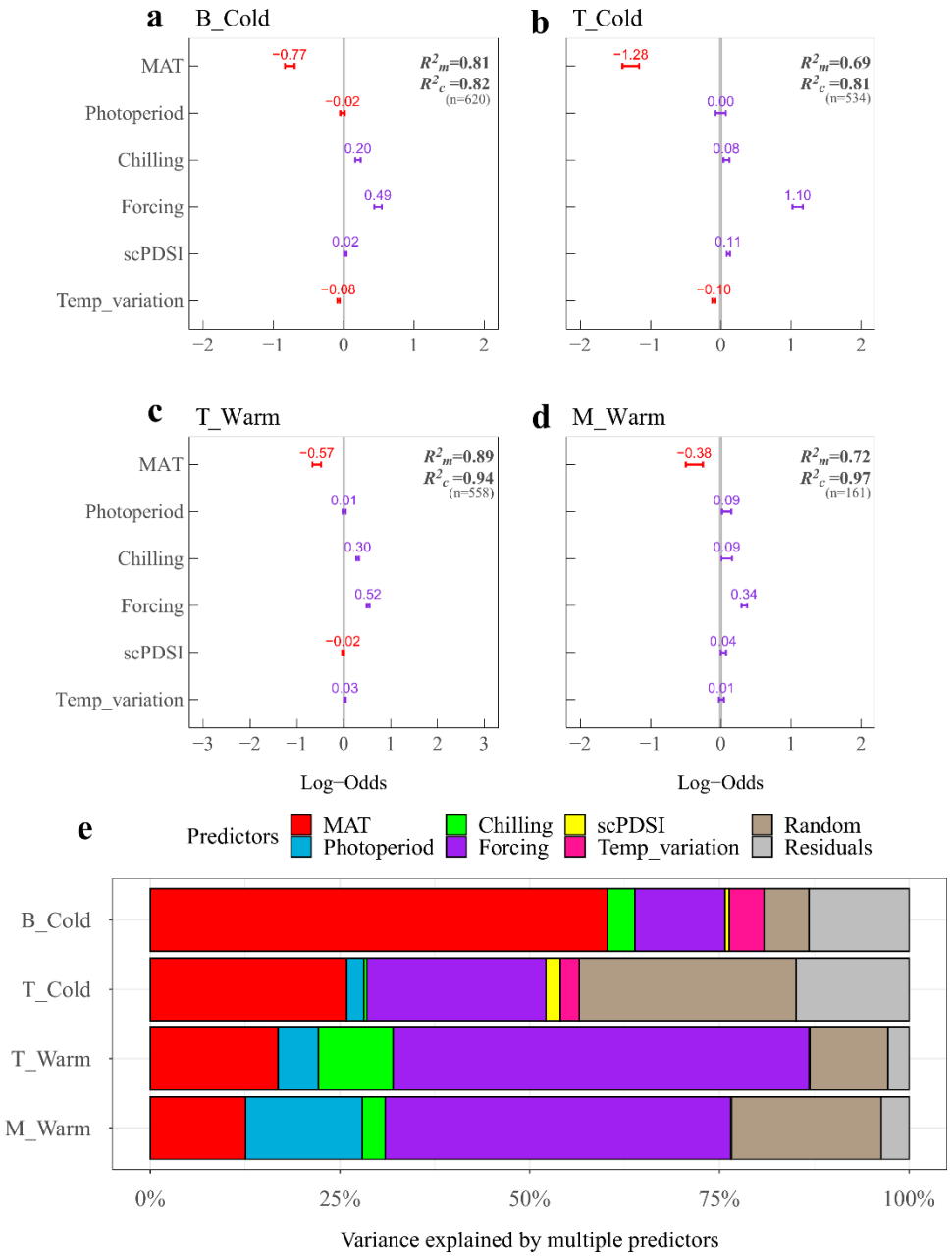

Figure S8: Summary of the direction and magnitude of the effect of multiple predictors on cell-wall-thickening DOY (day of the year) in different biomes at cold or warm sites, as fitted by linear mixed effect models. The upper (a, b) and middle (c,d) panels were from cold and warm sites, respectively. Significant effects occur when no overlaps exist between the 95% error bars and zero; the blue and red colors denote the positive versus negative effects, respectively. Variance partitioning for each model indicating the relative importance of each predictor is also shown in

e, and the sample sizes for each model are reported. B_Cold: boreal sites excluded the few dots above 4.9 ℃; T_Cold: temperate sites with MAT below 4.9 ℃; T_Warm: temperate sites with MAT above 4.9 ℃; M_Warm: Mediterranean sites excluded the few dots with MAT below 4.9 ℃.

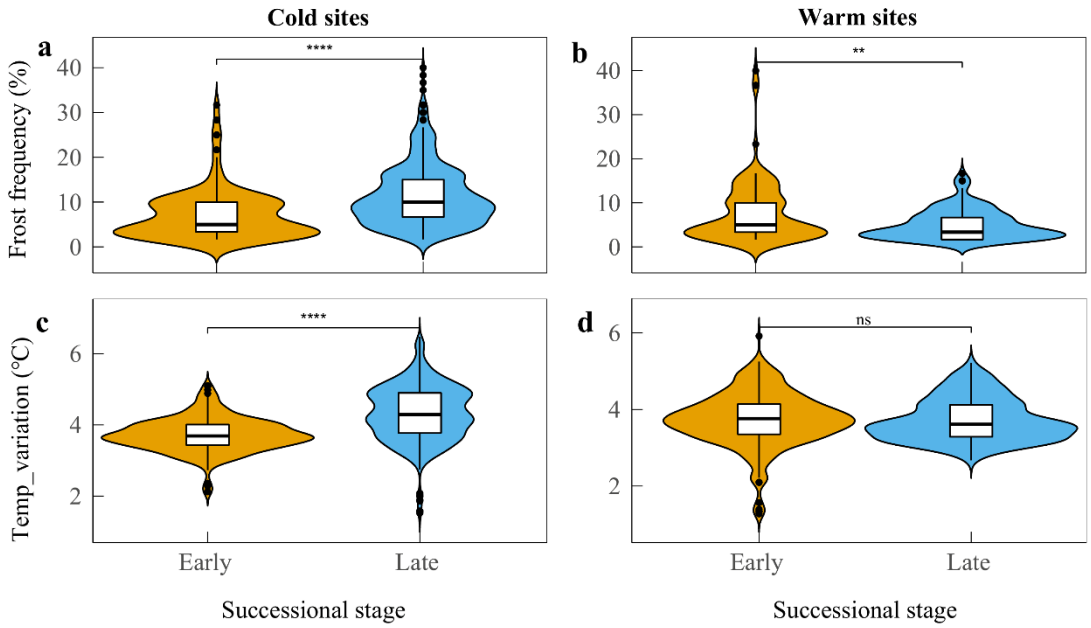

Figure S9: Variations (violin plots) and distributions (nested boxplots) of frost frequency and local spring temperature variation for early versus late successional species in the cold (a and c) and warm zones (b and d). Cold and warm sites were classified by the transition temperature at a mean annual temperature of MAT=4.9±1.1℃. E: early successional species; L: late successional species.

Tables S1-S4

Table S1: The sites, species, and years included in the analysis. The species were reported with the following acronyms and classified into early (E) and late (L) successional species type: ABAL, *Abies alba*, L; ABBA, *Abies balsamea*, L; ABGE, *Abies georgei*, L; CELI, *Cedrus libani*, L; JUPR, *Juniperus przewalskii*, E; JUTH, *Juniperus thurifera*, E; LADE, *Larix decidua*, E; PCAB, *Picea abies*, L; PCMA, *Picea mariana*, L; PICE, *Pinus cembra*, L; PIHA, *Pinus halepensis*, E; PIHE, *Pinus heldreichii*, E; PILE, *Pinus leucodermis*, E; PILO, *Pinus longaeva*, E; PIMA, *Pinus massoniana*, E; PIPE, *Pinus peuce*, E; PIPI, *Pinus pinaster*, E; PISY, *Pinus sylvestris*, E; PITA, *Pinus tabulaeformis*, E; and PIUN, *Pinus uncinata*, E. The entire study area was divided into subtropical (S), Mediterranean (M), temperate (T), and boreal (B) biomes. The site temperature for each site was computed as the average of the mean annual temperatures (MATs) across all years providing observations for the site. Sites with climate data obtained from nearby weather stations are indicated by *.

ID	Site	Biome	Latitude	Longitude	Altitude (m a.s.l.)	Study years	Species	Successional stage	Number of trees	Site temperature(°C)	References
DHS	CN-Dinghu Mountain	S	23°11'N	112°32'E	256	2015	PIMA	E	4	22.9	(Huang et al., 2018)
ZWY	CN-SCBG	S	23°11'N	113°22'E	23	2015-2016	PIMA	E	5	22.2	
SMT	CN-Shimentai	S	24°24'N	113°12'E	261	2015	PIMA	E	4	22.6	
SYG	CN-Sygera Mountain	T	29°39'N	94°42'E	3850	2007-2009	ABGE	L	5	4.5	(Li et al., 2013)
JGS	CN-Jigong Mountain	S	31°51'N	114°5'E	811	2014-2015	PIMA	E	3	16.2	(Zhang et al., 2017)
T2	TU-Cedar Research Forest	M	36°34'N	29°57'W	1960	2013	CELI	L	3	9.3	(Güney, Kerr, Sökücü, Zimmermann, & Küppers, 2015)
T4	TU-Cedar Research Forest	M	36°34'N	29°57'W	1055	2013	CELI	L	3	11.3	(Güney et al., 2015)
T1	TU-Cedar Research Forest	M	36°34'N	29°57'W	1665	2013	CELI	L	3	9.3	(Güney et al., 2015)
T3	TU-Cedar Research Forest	M	36°34'N	29°57'W	1355	2013	CELI	L	3	11.3	(Güney et al., 2015)
HSM	CN-Hasi Mountains	T	37°02'N	104°28'E	2456	2013-2014	PITA	E	9	5.9	(Zeng, Rossi, & Yang, 2018)
GUA	ES-Guardamar del Segura	M	38°06'N	0°39'W	15	2005	PIHA	E	6	19.5	(Rossi et al., 2016)
SDL	CN-Sidalong Forestry Station	T	38°27'N	99°56'E	3550	2013-2014	JUPR	E	9	-0.6	(Zeng et al., 2018)
MAI	ES-Maimó	M	38°31'N	0°38'W	845	2004-2005	PIHA	E	10	16.9	(Cuny et al., 2015)
SER	IT-Serra San Bruno	M	38°46'N	16°31'E	1008	2015	ABAL	L	5	11.4	(Antonucci, Rossi, Lombardi, Marchetti, & Tognetti,

ID	Site	Biome	Latitude	Longitude	Altitude (m a.s.l.)	Study years	Species	Successional stage	Number of trees	Site temperature(°C)	References
											2019)
JAR	ES	M	39°15'N	1°15'W	571	2005	PIHA	E	6	14.0	(Cuny et al., 2015)
JAN	ES	M	39°19'N	1°15'W	850	2004	PIHA	E	2	16.8	(Cuny et al., 2015)
POL	IT-Pollino	T	39°54'N	16°12'E	2053	2003-2004	PILE	E	10	3.6	(Deslauriers, Rossi, Anfodillo, & Saracino, 2008)
TCH	PT	M	40°22'N	8°49'W	15	2010-2014	PIPI	E	22	14.7	(Vieira et al., 2015)
VIL	ES-Villarroya de los Pinares	M	40°31'N	0°39'E	1690	2005	PISY	E	5	8.6	(J Julio Camarero, Guada, Sánchez-Salguero, & Cervantes, 2016)
TDR	BG-Bunderitsa valley	M	41°26'N	23°25'E	1780	2012-2014	PIHE, PIPE	E	10	5.5	(Cuny et al., 2015)
VRN	BG-Bunderitsa valley	M	41°27'N	23°15'E	1850	2012-2014	PIHE, PIPE	E	10	5.3	(Cuny et al., 2015)
PEN	ES-Peñaflor	M	41°47'N	0°58'W	340	2006-2010	JUTH, PIHA	E	27	15.7	(Jesús Julio Camarero, Olano, & Parras, 2010)
MYH	ES-Moncayo	M	41°47'N	0°43'W	1600	2011-2013	PISY	E	6	8.3	(Cuny et al., 2015)
MYL*	ES	M	41°47'N	1°49'W	1600	2011-2012	PISY	E	6	11.4	(Cuny et al., 2015)
PES	IT-Pescopennataro	T	41°52'N	14°30'E	1380	2015	ABAL	L	5	9.2	(Antonucci et

ID	Site	Biome	Latitude	Longitude	Altitude (m a.s.l.)	Study years	Species	Successional stage	Number of trees	Site temperature(°C)	References
											al., 2019)
SUS	IT-Val di Susa	T	45°3'N	6°40'E	2030	2003-2004	LADE, PICE, PIUN	E, L, E	15	4.0	(Rossi et al., 2006)
SAV*	IT-Lavazè	T	45°34'N	11°02'E	667	2010	PCAB	L	3	11	(Cocozza et al., 2016)
PAN	SI-Panska reka	T	46°0'N	14°40'E	400	2009-2012	PCAB	L	12	11.6	(Gričar et al., 2014)
LAV	IT-Lavaze	T	46°13'N	11°18'E	1776	2010	PCAB	L	3	2.4	(Rossi et al., 2016)
MEN	SI-Menina Planina	T	46°16'N	14°48'E	1200	2009-2012	PCAB	L	13	7.2	(Gričar et al., 2014)
N22	CH-Lötschental-N22	T	46°22'52''N	7°46'22''E	2182	2007-2010	LADE	E	4	2.2	(Cuny et al., 2019; Cuny et al., 2015)
N08	CH-Lötschental-N08	T	46°18'9''N	7°44'27''E	804	2008-2010	LADE, PCAB	E, L	8	9.3	(Cuny et al., 2019; Cuny et al., 2015)
N13d	CH-Lötschental-N13d	T	46°23'30''N	7°45'40''E	1361	2007-2013	LADE, PCAB	E, L	8	5.5	(Cuny et al., 2019; Cuny et al., 2015)
N13w	CH-Lötschental-N13w	T	46°23'36''N	7°45'50''E	1321	2013	LADE, PCAB	E, L	6	4.0	(Cuny et al., 2019; Cuny et al., 2015)
N16	CH-Lötschental-N16	T	46°23'14''N	7°45'52''E	1634	2007-2010	LADE, PCAB	E, L	8	4.9	(Cuny et al., 2019; Cuny et al., 2015)
N19	CH-Lötschental-N19	T	46°23'13''N	7°46'26''E	1961	2007-2010	LADE, PCAB	E, L	8	3.1	(Cuny et al., 2019; Cuny et al., 2015)
S16	CH-Lötschental-S16	T	46°23'50''N	7°45'19''E	1670	2007-2013	LADE, PCAB	E, L	8	4.8	(Cuny et al., 2019; Cuny et al., 2015)

ID	Site	Biome	Latitude	Longitude	Altitude (m a.s.l.)	Study years	Species	Successional stage	Number of trees	Site temperature(°C)	References
S19	CH-Lötschental-S19	T	46°23'48''N	7°44'45''E	1928	2007-2013	LADE, PCAB	E, L	8	3.7	(Cuny et al., 2019; Cuny et al., 2015)
S22	CH-Lötschental-S22	T	46°23'59''N	7°44'33''E	2104	2007-2013	LADE	E	4	3.1	(Cuny et al., 2019; Cuny et al., 2015)
SVT	IT-San Vito di Cadore	T	46°26'N	12°13'E	1000	2003	PCAB	L	1	8.0	(Anfodillo et al., 2012)
5T1	IT-Cinque Torri 1	T	46°27'N	12°8'E	2085	2001-2005	LADE, PCAB, PICE	E, L, L	23	2.4	(Rossi, Deslauriers, Anfodillo, & Carraro, 2007)
5T3	IT-Cinque Torri 3	T	46°27'N	12°8'E	2085	2004-2005	LADE, PCAB, PICE	E, L, L	15	1.8	(Rossi, Deslauriers, Anfodillo, & Carrer, 2008)
5T2	IT-Cinque Torri 2	T	46°28'N	12°8'E	2156	2002-2005	LADE, PCAB, PICE	E, L, L	12	2.3	(Rossi et al., 2007)
BOR	IT-Borca di Cadore	T	46°44'N	12°19'E	1150	2015	ABAL	L	5	8.1	(Antonucci et al., 2019)
TIM	AT-Patscherkofel-timberline	T	47°12'N	11°27'E	1950	2007	PICE	L	6	3.7	(Gruber, Wieser, & Oberhuber, 2009)
TRE	AT-Patscherkofel-treeline	T	47°12'N	11°27'E	2110	2007	PICE	L	4	2.4	(Gruber et al., 2009)
KRU	AT-Patscherkofel-krummholz	T	47°12'N	11°27'E	2180	2007	PICE	L	5	1.5	(Gruber et al., 2009)
DRY	AT-Tschirgant dry-mesic	T	47°14'N	10°50'E	750	2010-2011	LADE, PCAB, PISY	E, L, E	29	9.0	(Gričar et al., 2014)
SIM2	CA-Simoncouche2	B	48°12'N	71°14'W	350	2010-2011	ABBA, PCMA	L	12	2.6	(Lemay, Krause, Rossi,

ID	Site	Biome	Latitude	Longitude	Altitude (m a.s.l.)	Study years	Species	Successional stage	Number of trees	Site temperature(°C)	References
											& Achim, 2017)
SIM	CA-Simoncouche	B	48°13'N	71°15'W	338	2005-2014	ABBA, PCMA	L	55	2.4	(Rossi, Morin, Deslauriers, & PLOURDE, 2011)
ABR	FR-Abreschviller	T	48°21'N	7°4'E	430	2007-2009	ABAL, PCAB, PISY	L, L, E	16	9.2	(Rathgeber, Rossi, & Bontemps, 2011)
WAL	FR-Walscheid	T	48°22'N	7°5'E	370	2007-2009	ABAL, PCAB, PISY	L, L, E	16	10.3	(Rathgeber, Rossi, et al., 2011)
ARV	CA-Arvida	B	48°26'N	71°9'W	80	1999-2000	ABBA	L	18	3.7	(Rossi et al., 2006)
GRA	FR- Grandfontaine	T	48°28'N	4°08'E	650	2007-2008	ABAL, PCAB, PISY	L, L, E	15	8.2	(Rathgeber, Rossi, et al., 2011)
GRD	FR-Grandfontaine	T	48°29'N	7°9'E	643	2007-2009	ABAL, PCAB, PISY	L, L, E	15	8.6	(Rathgeber, Rossi, et al., 2011)
AMA	FR-Amance forest	T	48°44'52''N	6°19'30''E	270	2006-2007	ABAL, PISY	L, E	45	10.5	(Rathgeber, Longuetaud, Mothe, Cuny, & Le Moguédec, 2011; Taylor & Cooper, 2007)
AMA*	FR-Amance forest	T	48°44'52''N	6°19'30''E	270	2013-2014	PILO	E	16	10.4	(Taylor & Cooper, 2007)
BER	CA-Bernatchez	B	48°51'N	70°20'W	611	2002-2014	PCMA	L	31	0.5	(Rossi et al., 2011)

ID	Site	Biome	Latitude	Longitude	Altitude (m a.s.l.)	Study years	Species	Successional stage	Number of trees	Site temperature(°C)	References
SOB*	CZ-Brno	T	49°09'N	16°22'W	404	2013-2014	PISY	E	6	10.5	(Deslauriers, Morin, & Begin, 2003)
RAJ	CZ-Drahany highland	T	49°26'N	16°41'W	620	2009-2011	PCAB	L	6	8.1	(Gričar et al., 2014)
MIS	CA-Mistassibi	B	49°43'N	71°56'W	342	2002-2014	PCMA	L	28	1.1	(Rossi et al., 2011)
O1	DE-Bayreuth	T	49°55'N	11°35'W	355	2013	CELI	L	3	8.2	(Güney et al., 2015)
L23	CA-Liberal 23	B	49°58'N	72°30'W	380	1998-2000	ABBA	L	10	1.5	(Treml, Kašpar, Kuželová, & Gryc, 2015)
L24	CA-Liberal 24	B	49°58'N	72°30'W	430	1998-2001	ABBA	L	20	1.0	(Treml et al., 2015)
DAN	CA-Camp Daniel	B	50°41'N	72°11'W	487	2002-2014	PCMA	L	25	-0.7	(Lemay et al., 2017)
LH1	CZ-Lucní Hora-timberline	T	50°43'N	15°40'E	1310	2010-2012	PCAB	L	10	3.4	(Treml, Hejda, & Kašpar, 2019)
LH2	CZ-Lucní Hora-treeline	T	50°43'N	15°41'E	1450	2010-2012	PCAB	L	10	1.8	(Treml et al., 2019)
BLS	CZ-Bílé Labe Valley north	T	50°44'N	15°39'E	1270	2013-2014	PCAB	L	8	3.9	(Cuny et al., 2019; Cuny et al., 2015)
BLJ	CZ-Bílé Labe Valley south	T	50°44'N	15°39'E	1270	2013-2014	PCAB	L	8	4.2	(Cuny et al., 2019; Cuny et al., 2015)
SISE	CZ-Maly Sisak east	T	50°45'N	15°39'E	1375	2014-2015	PCAB	L	8	4.2	(Rossi, Girard, & Morin, 2014)
SISW	CZ-Maly Sisak west	T	50°46'N	15°38'E	1360	2014-2015	PCAB	L	8	4.1	(Rossi et al., 2014)

ID	Site	Biome	Latitude	Longitude	Altitude (m a.s.l.)	Study years	Species	Successional stage	Number of trees	Site temperature(°C)	References
MIR1	CA-Mirage	B	53°47'N	72°52'W	384	2012-2014	PCMA	L	10	-3.1	(Mäkinen, Jyske, & Nöjd, 2018)
RUO*	FI-Ruotsinkylä	B	60°12'N	25°0'E	60	2008-2010	PCAB, PISY	L, E	15	5.6	(Jyske, Kalliokoski, Mäkinen, & Nöjd, 2013)
HYY*	FI-Hyytiälä	B	61°53'N	24°18'E	181	2008	PCAB, PISY	L, E	6	4.9	(Jyske, Mäkinen, Kalliokoski, & Nöjd, 2014)
KIV*	FI-Kivalo	B	66°12'N	26°23'E	140	2009	PCAB	L	5	1.1	(Jyske et al., 2014)

Table S2. Descriptive summary statistics of cell-wall-thickening DOY (day of year) for all observations, for observations at cold sites, and for observations at warm sites.

	Cell-wall-thickening DOY		
Summary statistic	All data	Cold	Warm
Mean (DOY)	156.4	166.6	142
Median (DOY)	159	167	141
5% quantile (DOY)	120	147	105
95% quantile (DOY)	187	187	179
Minimum (DOY)	15	120	15
Maximum (DOY)	221	212	221
Intercept ± S.E. mixed model	150.72 ± 6.22	163.74 ± 2.77	143.59 ± 8.02
t-value	24.23	59.11	17.91
P-value	< 0.001	< 0.001	< 0.001

Table S3. Summary of linear mixed modeling of the effects of selected predictors on cell-wall-thickening DOY (day of year); CI: confidence interval.

	Model selection					Fixed effect of the selected model			
Models	**Fixed-effect structure***	**Effect dropped**	**ΔAIC$_c$†**	**Weight**	***P*-value‡**	**Component**	**Coefficient**	**90% CI**	**95% CI**
All	MAT+Photoperiod+Chilling+Forcing+scPDSI+Temp_variation		0	1		(Intercept)	20.70	6.59, 35.07	3.85, 37.79
	MAT+Photoperiod+Forcing+scPDSI+Temp_variation	Chilling	263.46	0	<0.001	Chilling	0.162	0.146, 0.177	0.143, 0.180
	MAT+Photoperiod+Chilling+Forcing+Temp_variation	scPDSI	354.95	0	<0.001	scPDSI	0.85	0.689, 1.012	0.658, 1.043
	MAT+Photoperiod+Chilling+Forcing+scPDSI	Temp_variation	368.28	0	<0.001	Temp_variation	-2.18	-2.60, -1.76	-2.68, -1.68
	MAT+Chilling+Forcing+scPDSI+Temp_variation	Photoperiod	431.86	0	<0.001	Photoperiod	8.79	7.87, 9.68	7.70, 9.85
	Photoperiod+Chilling+Forcing+scPDSI+Temp_variation	MAT	752.32	0	<0.001	MAT	-4.92	-5.18, -4.65	-5.24, -4.60
	MAT+Photoperiod+Chilling+scPDSI+Temp_variation	Forcing	1670.26	0	<0.001	Forcing	0.065	0.063, 0.067	0.063, 0.068
Cold	**Selected model:** MAT+Photoperiod+Chilling+Forcing+scPDSI+Temp_variation								
	MAT+Photoperiod+Chilling+Forcing+scPDSI+Temp_variation		0	0.681		(Intercept)	155.0	150.4, 159.6	149.6, 160.6
	MAT+Chilling+Forcing+scPDSI+Temp_variation	Photoperiod	1.51	0.319	0.1485				
	MAT+Photoperiod+Chilling+Forcing+Temp_variation	scPDSI	32.5	0	<0.001	scPDSI	0.826	0.618, 1.032	0.579, 1.071
	MAT+Photoperiod+Chilling+Forcing+scPDSI	Temp_variation	59.05	0	<0.001	Temp_variation	-2.66	-3.22, -2.11	-3.32, -2.00
	MAT+Photoperiod+Forcing+scPDSI+Temp_variation	Chilling	92.2	0	<0.001	Chilling	0.156	0.132, 0.182	0.127, 0.187
	MAT+Photoperiod+Chilling+scPDSI+Temp_variation	Forcing	545.28	0	<0.001	Forcing	0.097	0.091, 0.103	0.090, 0.104
	Photoperiod+Chilling+Forcing+scPDSI+Temp_variation	MAT	548.84	0	<0.001	MAT	-6.66	-7.06, -6.24	-7.14, -6.17
Warm	**Selected model**: MAT+Chilling+Forcing+scPDSI+Temp_variation								
	MAT+Photoperiod+Chilling+Forcing+scPDSI+Temp_variation		0	1		(Intercept)	-36.19	-49.43, -22.76	-51.99, -20.20
	Photoperiod+Chilling+Forcing+scPDSI+Temp_variation	MAT	112.1	0	<0.001	MAT	-2.81	-3.21, -2.41	-3.29, -2.33
	MAT+Photoperiod+Chilling+Forcing+scPDSI	Temp_variation	128.81	0	0.0484	Temp_variation	0.75	0.127, 1.375	0.0068, 1.495
	MAT+Photoperiod+Chilling+Forcing+Temp_variation	scPDSI	271.18	0	0.0036	scPDSI	0.44	0.190, 0.684	0.142, 0.732
	MAT+Photoperiod+Forcing+scPDSI+Temp_variation	Chilling	275.18	0	<0.001	Chilling	0.22	0.196, 0.234	0.193, 0.238

	MAT+Chilling+Forcing+scPDSI+Temp_variation	Photoperiod	504.85	0	<0.001	Photoperiod	10.62	9.80, 11.42	9.649, 11.581
	MAT+Photoperiod+Chilling+scPDSI+Temp_variation	Forcing	1151.35	0	<0.001	Forcing	0.060	0.0578, 0.0615	0.0574, 0.0619
	Selected model: MAT+Photoperiod+Chilling+Forcing+scPDSI+Temp_variation								
Early_Cold	MAT+Photoperiod+Forcing+scPDSI+Temp_variation	Chilling	0	0.823	0.045	(Intercept)	333.6	282.00, 382.65	273.16, 393.80
	MAT+Photoperiod+Chilling+Forcing+scPDSI+Temp_variation		3.07	0.177		Chilling	0.0623	0.0124, 0.112	0.00273, 0.122
	MAT+Chilling+Forcing+scPDSI+Temp_variation	Photoperiod	23.39	0	<0.001	Photoperiod	-8.4	-11.45, -5.25	-12.13, -4.69
	MAT+Photoperiod+Chilling+Forcing+Temp_variation	scPDSI	43.73	0	<0.001	scPDSI	2.786	2.070, 3.414	1.940, 3.543
	MAT+Photoperiod+Chilling+Forcing+scPDSI	Temp_variation	61.11	0	<0.001	Temp_variation	-5.93	-7.40, -4.21	-7.70, -3.90
	MAT+Photoperiod+Chilling+scPDSI+Temp_variation	Forcing	167.42	0	<0.001	Forcing	0.1131	0.102, 0.125	0.100, 0.128
	Photoperiod+Chilling+Forcing+scPDSI+Temp_variation	MAT	181.72	0	<0.001	MAT	-12	-13.17, -10.61	-13.42, -10.37
	Selected model: MAT+Photoperiod+Chilling+Forcing+scPDSI+Temp_variation								
Early_Warm	MAT+Photoperiod+Chilling+Forcing+Temp_variation	scPDSI	0	0.53	0.166				
	MAT+Photoperiod+Chilling+Forcing	scPDSI+ Temp_variation	1.22	0.288		(Intercept)	-83.19	-105.55, -59.78	-109.94, -55.36
	MAT+Photoperiod+Chilling+Forcing+scPDSI	Temp_variation	2.14	0.182	0.098				
	Photoperiod+Chilling+Forcing+scPDSI+Temp_variation	MAT	35.08	0	<0.001	MAT	-2.369	-2.99, -1.75	-3.11, -1.626
	MAT+Photoperiod+Forcing+scPDSI+Temp_variation	Chilling	39.24	0	<0.001	Chilling	0.1472	0.116, 0.178	0.110, 0.184
	MAT+Chilling+Forcing+scPDSI+ Temp_variation	Photoperiod	203.5	0	<0.001	Photoperiod	14.29	12.86, 15.64	12.59, 15.91
	MAT+Photoperiod+Chilling+scPDSI+Temp_variation	Forcing	437.08	0	<0.001	Forcing	0.04795	0.0453, 0.0507	0.0448, 0.0512
	Selected model: MAT+Photoperiod+Chilling+Forcing								
Late_Cold	MAT+Photoperiod+Chilling+Forcing+scPDSI+Temp_variation		0	0.959		(Intercept)	35.28	0.212, 72.820	-6.950, 79.413
	MAT+Photoperiod+Chilling+Forcing+Temp_variation	scPDSI	6.31	0.041	0.001	scPDSI	0.4131	0.208, 0.623	0.168, 0.663
	MAT+Chilling+Forcing+scPDSI+Temp_variation	Photoperiod	56.1	0	<0.001	Photoperiod	7.584	5.222, 9.774	4.807, 10.220
	MAT+Photoperiod+Forcing+scPDSI+Temp_variation	Chilling	74.22	0	<0.001	Chilling	0.1474	0.122, 0.174	0.117, 0.179
	MAT+Photoperiod+Chilling+Forcing+scPDSI	Temp_variatio	250.39	0	<0.00	Temp_variatio	-3.081	-3.63, -2.53	-3.739, -2.427

		n			1	n			
	MAT+Photoperiod+Chilling+scPDSI+Temp_variation	Forcing	365.98	0	<0.001	Forcing	0.0811	0.0750, 0.0874	0.0738, 0.0886
	Photoperiod+Chilling+Forcing+scPDSI+Temp_variation	MAT	465.5	0	<0.001	MAT	-5.98	-6.38, -5.58	-6.46, -5.51
	Selected model: MAT+Photoperiod+Chilling+Forcing+scPDSI+Temp_variation								
Late_Warm	MAT+Photoperiod+Chilling+Forcing+Temp_variation	scPDSI	0	0.759	0.0822	(Intercept)	-85.62	-101.14, -69.73	-104.17, -66.71
	MAT+Photoperiod+Chilling+Forcing+scPDSI+Temp_variation		2.29	0.241					
	MAT+Photoperiod+Chilling+Forcing+scPDSI	Temp_variation	24.28	0	<0.001	Temp_variation	1.937	1.286, 2.581	1.161, 2.706
	Photoperiod+Chilling+Forcing+scPDSI+Temp_variation	MAT	82	0	<0.001	MAT	-3.177	-3.668, -2.684	-3.763, -2.589
	MAT+Photoperiod+Forcing+scPDSI+Temp_variation	Chilling	261.15	0	<0.001	Chilling	0.23	0.212, 0.248	0.208, 0.252
	MAT+Chilling+Forcing+scPDSI+Temp_variation	Photoperiod	273.52	0	<0.001	Photoperiod	13.38	12.36, 14.36	12.167, 14.547
	MAT+Photoperiod+Chilling+scPDSI+Temp_variation	Forcing	490.33	0	<0.001	Forcing	0.0609	0.0581, 0.0637	0.0576, 0.0643
	Selected model: MAT+Photoperiod+Chilling+Forcing+Temp_variation								

*The structure of the fixed-effects model component was examined through a backward stepwise procedure, starting with a maximal model (M) with all the six candidate fixed covariates.
†Second-order ΔAIC means the Akaike Information Criterion difference relative to the most complex model.
‡Significance of the likelihood ratio test.

Table S4: Variance inflation factor (vif) of each predictor variable in the linear mixed models for all observations and subset modelings corresponding to the results shown in Fig. 3.

Models	Predictors					
	MAT	Photoperiod	Chilling	Forcing	scPDSI	Temp_variation
vif(mod_all)	1.142	1.093	1.070	1.153	1.117	1.086
vif(mod_Cold_sites)	1.231	1.066	1.173	1.209	1.284	1.383
vif(mod_Warm_sites)	1.260	1.136	1.266	1.164	1.200	1.095
vif(mod_Early_Cold)	1.246	1.377	1.359	1.465	1.359	1.354
vif(mod_Early_Warm)	1.471	1.087	1.625	1.160	1.347	1.083
vif(mod_Late_Cold)	1.297	1.157	1.175	1.285	1.405	1.510
vif(mod_Late_Warm)	1.573	2.020	1.498	1.932	1.591	1.238
vif(mod_B_Cold)	1.295	1.042	1.197	1.353	1.513	1.894
vif(mod_T_Cold)	1.245	1.046	1.321	1.129	1.227	1.219
vif(mod_T_Warm)	1.500	1.263	1.280	1.367	1.475	1.184
vif(mod_M_Warm)	2.455	1.889	2.186	2.669	1.393	1.429

References

Anfodillo, T., Deslauriers, A., Menardi, R., Tedoldi, L., Petit, G., & Rossi, S. (2012). Widening of xylem conduits in a conifer tree depends on the longer time of cell expansion downwards along the stem. *Journal of experimental botany, 63*(2), 837-845.

Antonucci, S., Rossi, S., Lombardi, F., Marchetti, M., & Tognetti, R. (2019). Influence of climatic factors on silver fir xylogenesis along the Italian Peninsula. *Iawa Journal, 40*(2), 259-S253.

Camarero, J. J., Guada, G., Sánchez-Salguero, R., & Cervantes, E. (2016). Winter drought impairs xylem phenology, anatomy and growth in Mediterranean Scots pine forests. *Tree Physiology, 36*(12), 1536-1549.

Camarero, J. J., Olano, J. M., & Parras, A. (2010). Plastic bimodal xylogenesis in conifers from continental Mediterranean climates. *New Phytologist, 185*(2), 471-480.

Cleland, E. E., Chuine, I., Menzel, A., Mooney, H. A., & Schwartz, M. D. (2007). Shifting plant phenology in response to global change. *Trends in ecology & evolution, 22*(7), 357-365.

Cocozza, C., Palombo, C., Tognetti, R., La Porta, N., Anichini, M., Giovannelli, A., & Emiliani, G. (2016). Monitoring intra-annual dynamics of wood formation with microcores and dendrometers in Picea abies at two different altitudes. *Tree Physiology, 36*(7), 832-846.

Cuny, H. E., Fonti, P., Rathgeber, C. B., von Arx, G., Peters, R. L., & Frank, D. C. (2019). Couplings in cell differentiation kinetics mitigate air temperature influence on conifer wood anatomy. *Plant, Cell & Environment, 42*(4), 1222-1232.

Cuny, H. E., Rathgeber, C. B., Frank, D., Fonti, P., Mäkinen, H., Prislan, P., . . . Vavrčík, H. (2015). Woody biomass production lags stem-girth increase by over one month in coniferous forests. *Nature Plants, 1*(11), 1-6.

Deslauriers, A., Morin, H., & Begin, Y. (2003). Cellular phenology of annual ring formation of Abies balsamea in the Quebec boreal forest (Canada). *Canadian Journal of Forest Research, 33*(2), 190-200.

Deslauriers, A., Rossi, S., Anfodillo, T., & Saracino, A. (2008). Cambial phenology, wood formation and temperature thresholds in two contrasting years at high altitude in southern Italy. *Tree Physiology, 28*(6), 863-871.

Frey, S. J., Hadley, A. S., Johnson, S. L., Schulze, M., Jones, J. A., & Betts, M. G. (2016). Spatial models reveal the microclimatic buffering capacity of old-growth forests. *Science advances, 2*(4), e1501392.

Fu, Y. H., Zhao, H., Piao, S., Peaucelle, M., Peng, S., Zhou, G., . . . Peñuelas, J. (2015). Declining global warming effects on the phenology of spring leaf unfolding. *Nature, 526*(7571), 104-107.

Gričar, J., Čufar, K., Oven, P., & Schmitt, U. (2005). Differentiation of terminal latewood tracheids in silver fir trees during autumn. *Annals of Botany, 95*(6), 959-965.

Gričar, J., Prislan, P., Gryc, V., Vavrčík, H., De Luis, M., & Čufar, K. (2014). Plastic and locally adapted phenology in cambial seasonality and production of xylem and phloem cells in Picea abies from temperate environments. *Tree Physiology, 34*(8), 869-881.

Gruber, A., Wieser, G., & Oberhuber, W. (2009). Intra-annual dynamics of stem CO2 efflux in relation to cambial activity and xylem development in Pinus cembra. *Tree Physiology, 29*(5), 641-649.

Güney, A., Kerr, D., Sökücü, A., Zimmermann, R., & Küppers, M. (2015). Cambial activity and xylogenesis in stems of Cedrus libani A. Rich at different altitudes. *Botanical studies, 56*(1), 20.

Hänninen, H. (1990). Modelling bud dormancy release in trees from cool and temperate regions.

Huang, J.-G., Guo, X., Rossi, S., Zhai, L., Yu, B., Zhang, S., & Zhang, M. (2018). Intra-annual wood formation of subtropical Chinese red pine shows better growth in dry season than wet season. *Tree Physiology, 38*(8), 1225-1236.

Huang, J.-G., Ma, Q., Rossi, S., Biondi, F., Deslauriers, A., Fonti, P., & Liang, E. (2020). Photoperiod and temperature as dominant environmental drivers triggering secondary growth resumption in Northern Hemisphere conifers. *Proceedings of the National Academy of Sciences, 117*(34), 20645-20652.

Jyske, T., Kalliokoski, T., Mäkinen, H., & Nöjd, P. (2013). *Intra-annual xylem formation of Norway spruce and Scots pine across latitudinal gradient in Finland.* Paper presented at the Proceedings of the International Symposium on Wood Structure in Plant Biology and Ecology, 17-20 April, 2013, Naples, Italy/Ed. Arena, C., Battipaglia, G., Cherubini, P., De Micco, V. & Sass-Klaassen, U.

Jyske, T., Mäkinen, H., Kalliokoski, T., & Nöjd, P. (2014). Intra-annual tracheid production of Norway spruce and Scots pine across a latitudinal gradient in Finland. *Agricultural and Forest Meteorology, 194*, 241-254.

Lemay, A., Krause, C., Rossi, S., & Achim, A. (2017). Xylogenesis in stems and roots after thinning in the boreal forest of Quebec, Canada. *Tree Physiology, 37*(11), 1554-1563.

Li, X., Liang, E., Gričar, J., Prislan, P., Rossi, S., & Čufar, K. (2013). Age dependence of xylogenesis and its climatic sensitivity in Smith fir on the south-eastern Tibetan Plateau. *Tree Physiology, 33*(1), 48-56.

Mäkinen, H., Jyske, T., & Nöjd, P. (2018). Dynamics of diameter and height increment of Norway spruce and Scots pine in southern Finland. *Annals of Forest Science, 75*(1), 28.

Murray, M., Cannell, M., & Smith, R. (1989). Date of budburst of fifteen tree species in Britain following climatic warming. *Journal of Applied Ecology*, 693-700.

Poulter, B., Aragão, L., Andela, N., Bellassen, V., Ciais, P., Kato, T., . . . Pederson, N. (2019). The global forest age dataset and its uncertainties (GFADv1. 1). *NASA National Aeronautics and Space Administration, PANGAEA.*

Rathgeber, C. B., Longuetaud, F., Mothe, F., Cuny, H., & Le Moguédec, G. (2011). Phenology of wood formation: data processing, analysis and visualisation using R (package CAVIAR). *Dendrochronologia, 29*(3), 139-149.

Rathgeber, C. B., Rossi, S., & Bontemps, J.-D. (2011). Cambial activity related to tree size in a mature silver-fir plantation. *Annals of Botany, 108*(3), 429-438.

Rossi, S., Anfodillo, T., Čufar, K., Cuny, H. E., Deslauriers, A., Fonti, P., . . . Huang, J. G. (2016). Pattern of xylem phenology in conifers of cold ecosystems at the Northern Hemisphere. *Global Change Biology, 22*(11), 3804-3813.

Rossi, S., Deslauriers, A., Anfodillo, T., & Carraro, V. (2007). Evidence of threshold temperatures for xylogenesis in conifers at high altitudes. *Oecologia, 152*(1), 1-12.

Rossi, S., Deslauriers, A., Anfodillo, T., & Carrer, M. (2008). Age‐dependent xylogenesis in timberline conifers. *New Phytologist, 177*(1), 199-208.

Rossi, S., Deslauriers, A., Anfodillo, T., Morin, H., Saracino, A., Motta, R., & Borghetti, M. (2006). Conifers in cold environments synchronize maximum growth rate of tree‐ring formation with day length. *New Phytologist, 170*(2), 301-310.

Rossi, S., Girard, M. J., & Morin, H. (2014). Lengthening of the duration of xylogenesis engenders disproportionate increases in xylem production. *Global Change Biology, 20*(7), 2261-2271.

Rossi, S., Morin, H., Deslauriers, A., & PLOURDE, P. Y. (2011). Predicting xylem phenology in black spruce under climate warming. *Global Change Biology, 17*(1), 614-625.

Taylor, A., & Cooper, P. (2007). The effect of stem girdling on wood quality. *Wood and fiber science, 34*(2), 212-220.

Treml, V., Hejda, T., & Kašpar, J. (2019). Differences in growth between shrubs and trees: How does the stature of woody plants influence their ability to thrive in cold regions? *Agricultural and Forest Meteorology, 271*, 54-63.

Treml, V., Kašpar, J., Kuželová, H., & Gryc, V. (2015). Differences in intra-annual wood formation in Picea abies across the treeline ecotone, Giant Mountains, Czech Republic. *Trees, 29*(2), 515-526.

Vieira, J., Campelo, F., Rossi, S., Carvalho, A., Freitas, H., & Nabais, C. (2015). Adjustment capacity of maritime pine cambial activity in drought-prone environments. *PLoS One, 10*(5), e0126223.

Wang, H., Wu, C., Ciais, P., Peñuelas, J., Dai, J., Fu, Y., Ge Q.. Overestimation of the effect of climatic warming on spring phenology due to misrepresentation of chilling. Nat Commun 11, 4945 (2020). https://doi.org/10.1038/s41467-020-18743-8

Wang, T., Ottlé, C., Peng, S., Janssens, I. A., Lin, X., Poulter, B., . . . Ciais, P. (2014). The influence of local spring temperature variance on temperature sensitivity of spring phenology. *Global Change Biology, 20*(5), 1473-1480.

Way, D. A., & Montgomery, R. A. (2015). Photoperiod constraints on tree phenology, performance and migration in a warming world. *Plant, Cell & Environment, 38*(9), 1725-1736.

Zeng, Q., Rossi, S., & Yang, B. (2018). Effects of age and size on xylem phenology in two conifers of northwestern China. *Frontiers in Plant Science, 8*, 2264.

Zhang, S., Huang, J.-G., Rossi, S., Ma, Q., Yu, B., Zhai, L., . . . Zhang, W. (2017). Intra-annual dynamics of xylem growth in Pinus massoniana submitted to an experimental nitrogen addition in Central China. *Tree Physiology, 37*(11), 1546-1553.